Coordination Chemistry Reviews 253 (2009) 3042–3066

Contents lists available at ScienceDirect

Coordination Chemistry Reviews

journal homepage: www.elsevier.com/locate/ccr

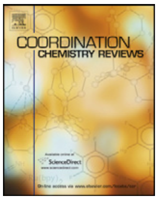

Review

Potential applications of metal-organic frameworks

Ryan J. Kuppler[a], Daren J. Timmons[b], Qian-Rong Fang[a], Jian-Rong Li[a], Trevor A. Makal[a], Mark D. Young[a], Daqiang Yuan[a], Dan Zhao[a], Wenjuan Zhuang[a], Hong-Cai Zhou[a,*]

[a] *Department of Chemistry, Texas A&M University, PO Box 30012, College Station, TX 77842-3012, United States*
[b] *Department of Chemistry, Virginia Military Institute, 303 Science Hall, Lexington, VA 24450, United States*

Contents

---

[*] Corresponding author. Tel.: +1 979 845 4034.

doi:10.1016/j.ccr.2009.05.019

A R T I C L E I N F O

Article history:
Received 16 January 2009
Accepted 25 May 2009
Available online 28 June 2009

Keywords:
Metal-organic frameworks
Structure
Potential applications
Applications
Porous materials

A B S T R A C T

Metal-organic frameworks have received much attention in recent years especially as newly developed porous materials. As such, they possess a wide array of potential applications including materials for gas storage, gas/vapor separation, catalysis, luminescence, and drug delivery. In the review, these potential applications of metal-organic frameworks are examined and an outlook will be proposed.

1. Introduction

Porous materials are very useful in gas storage, adsorption-based gas/vapor separation, shape/size-selective catalysis, drug storage and delivery, and as templates in the preparation of low-dimensional materials [1–6]. Traditionally, porous materials have been either organic or inorganic materials. Perhaps the most common organic porous material is activated carbon. These are usually prepared by pyrolysis of carbon-rich materials, have high surface areas and high adsorption capacities, yet do not possess ordered structures. Despite this lack of order, porous carbon materials have many uses, including the separation and storage of gases, the purification of water, and solvent removal and recovery [7].

Inorganic porous frameworks possess highly ordered structures (*e.g.* zeolites). Syntheses often require an inorganic or organic template with strong interactions forming between the inorganic framework and the template during the synthesis. As a consequence, removal of the template can result in collapse of the framework. Inorganic frameworks also suffer from a lack of diversity, as the variation of elements used seldom deviates from Al, Si and chalcogens. Nevertheless, inorganic frameworks have been useful in separation and catalysis applications [3].

In order to take advantage of the properties of both organic and inorganic porous materials, porous hybrids, known as metal-organic frameworks (MOFs), can be generated that are both stable and ordered and possess high surface areas. It should be noted that MOFs go by many names (porous coordination networks, porous coordination polymers, etc.) yet all refer to similar if not the same general type of materials. The difference in nomenclature merely reflects the type of framework and the researchers who constructed it. MOFs are essentially coordination polymers formed in the most elementary sense by connecting together metal ions with polytopic organic linkers often resulting in fascinating structural topologies. These materials have attracted a great deal of attention in the past decade, and the increase in the number of papers published in this area during recent years is remarkable (Fig. 1). Applications in gas storage, gas/vapor separation, size-, shape-, and enantio-selective catalysis, luminescent and fluorescent materials, and drug storage and delivery have been explored [8–10].

2. Synthesis and structure of MOFs

2.1. Synthetic routes to metal-organic frameworks

MOFs are typically synthesized by combining organic ligands and metal salts in solvothermal reactions at relatively low temperatures (below 300 °C). The characteristics of the ligand (bond angles, ligand length, bulkiness, chirality, etc.) play a crucial role in dictating what the resultant framework will be. Additionally, the tendency of metal ions to adopt certain geometries also influences the structure of the MOF. The reactants are mixed in high boiling, polar solvents such as water, dialkyl formamides, dimethyl sulfoxide or acetonitrile. The most important parameters of solvothermal MOF synthesis are temperature, the concentrations of metal salt and ligand (which can be varied across a large range), the extent of solubility of the reactants in the solvent, and the pH of the solution. Although experience often dictates the best conditions for growing these crystalline frameworks, experimentation and trial-and-error methods are still often necessary. Reviews which describe the synthesis and characterization of MOFs have been previously published [11–16].

In addition to this standard method, several other synthetic methodologies are described in the literature including the mixture of non-miscible solvents [17], an electrochemical route [18], and a high-throughput approach [19]. One of the most promising alternatives is microwave irradiation which allows access to a wide range of temperatures and can be used to shorten crystallization times while controlling face morphology and particle size distribution [12,20,21]. A serious limitation of this approach is the general lack of formation of crystals large enough to obtain good structural data.

2.2. Structural highlights of metal-organic frameworks

When considering the structure of MOFs, it is helpful to recognize the secondary building units (SBUs), which dictate the final topology of a framework. While the organic linkers are also important SBUs, their structure seldom changes during MOF assembly. The following discussion will focus on metal-cluster-based SBUs, which result from the initial bonding between the metal ions and

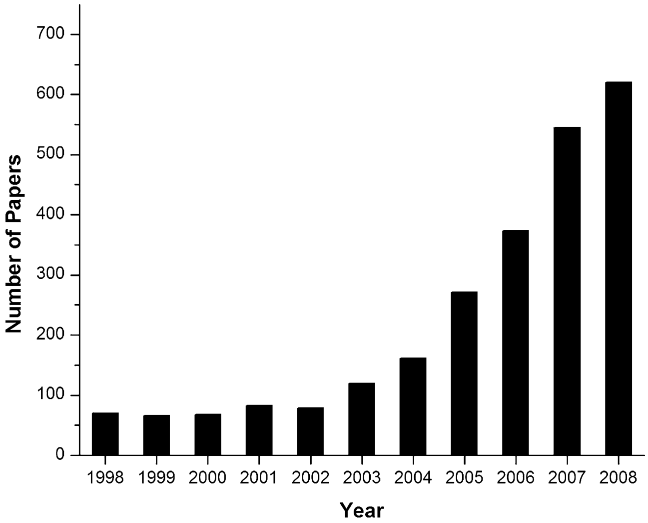

Fig. 1. Number of publications on MOFs over the past decade.

bridging ligands [16]. Fig. 2a and b shows SBUs with a trigonal and a square planar arrangement of the metal atoms, respectively. Fig. 2c features a tetrahedron of metal atoms surrounding a central oxo anion, and a dimetal paddlewheel SBU is shown in Fig. 2d. In each case, the edges between two metal ions are bridged by the coordinating atoms of the ligand and result in control of the orientation of the linker.

Recently, the geometry of the SBU has been proven to be dependent on not only the structure of the ligand and type of metal utilized, but also the metal to ligand ratio, the solvent, and the source of anions to balance the charge of the metal ion [22]. Several publications discussed the topic of SBU formation and structure in depth [16,23–26].

Pores are the void spaces formed within MOFs (or any porous materials) upon the removal of guest molecules (Fig. 3) [27]. In general, large pores are advantageous for conducting host–guest chemistry such as catalysis, therefore mesoporous (openings between 20 and 500 Å) or even macroporous (openings greater than 500 Å) materials are attractive. Microporous materials have pores less than 20 Å which result in strong interactions between gas molecules and the pore walls making them good candidates for gas storage and gas separation applications. In all cases, measurements of these openings are done from atom to atom while subtracting the van der Waals radii to give the space available for access by guest molecules.

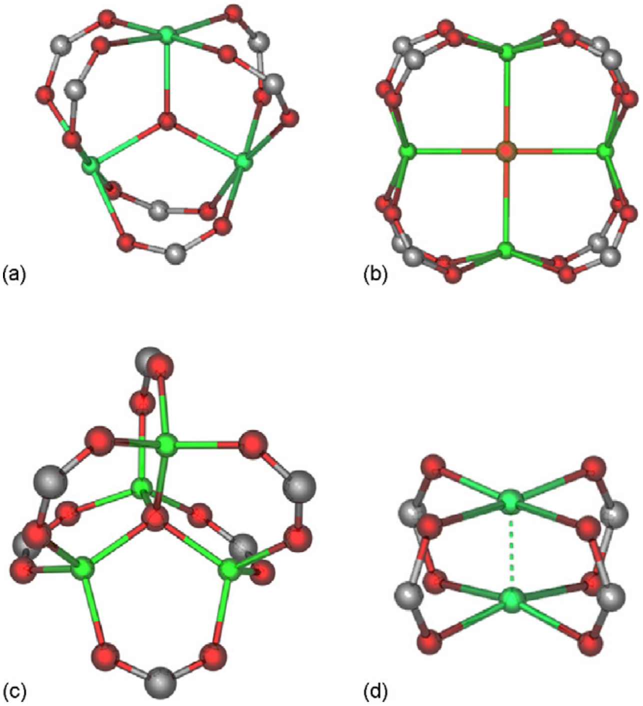

Fig. 2. Structural representations of several SBUs, including (a) trigonal planar, (b) square planar, (c) tetrahedral, and (d) tetragonal paddlewheel.

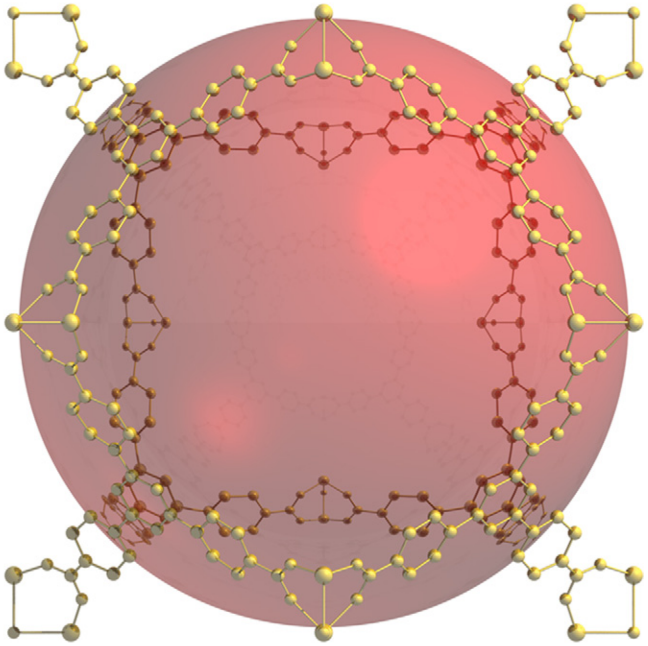

Fig. 3. Looking through the window created by the ligands into the pore (red sphere) of PCN-9 [28]. (For interpretation of the references to color in this figure legend, the reader is referred to the web version of the article.)

The pores of MOFs are usually occupied by solvent molecules that must be removed for most applications. Structural collapse can occur and, in general, the larger the pore, the more likely the collapse. Permanent porosity results when the framework remains intact and is more difficult to achieve in mesoporous MOFs than in microporous analogues.

Although MOFs can be constructed with ligands designed to generate large pores, frameworks will often interpenetrate one another to maximize packing efficiency [23]. In such cases, the pores sizes are greatly reduced, but this may be beneficial for some applications. Indeed interpenetrated frameworks have been intentionally formed and found to lead to improved performance, for example, in H_2 storage [29].

Following the synthesis, MOFs, like other coordination polymers, may participate in further chemical reactions to decorate the frameworks with molecules or functional groups in what is known as post-synthetic modification (PSM) [30]. Sometimes the presence of a certain functional group on a ligand prevents the formation of the targeted MOF. In this situation, it is necessary to first form a MOF with the desired topology, and then add the functional group to the framework. This may be applied to MOFs that are designed for catalysis and gas storage, as these applications require functional groups to modify the surface property and pore geometry. It is important to keep in mind that the two most important factors in PSM are making sure that the reagent used to enhance the functionality is small enough to fit inside the cavity of the MOF and that the reaction conditions will not destroy the framework. If the reagent is too small to enter the cavity or the framework is destroyed by the reaction, the modification will be useless.

3. Hydrogen and methane storage in MOFs

3.1. Introduction

A tank charged with a porous adsorbent enables a gas to be stored at a much lower pressure than an identical tank without an adsorbent. Thus, high pressure tanks and multi-stage compressors can be avoided providing a safer and more economical gas storage method. Many gas storage studies have been conducted on porous adsorbents such as activated carbon, carbon nanotubes, and zeolites [6]. MOFs have received growing attention as such adsorbents due to their tunable pore geometries and flexible frameworks. The need to reduce global reliance on fossil fuels by the use of alternative technologies has pushed hydrogen and methane gases to the forefront of gas storage applications. This section will review the state-of-the-art study of hydrogen and methane storage in MOFs.

3.2. Hydrogen storage in MOFs

Hydrogen is an ideal energy carrier. It almost triples the gravimetric heat of combustion of gasoline (120 MJ/kg *vs.* 44.5 MJ/kg) [31], and the main byproduct after energy release is water. This makes hydrogen a leading candidate for on-board fuel. However, hydrogen exists in a gaseous state at ambient temperature and pressure with a density of 0.08 kg/m^3. Even in its liquid state, which requires pressurizing at a very low temperature (20.27 K), the density can only reach 70.8 kg/m^3, one tenth of that of gasoline ($\sim$700 kg/m^3) [31]. This extremely low volumetric storage density presents a hurdle for the practical usage of hydrogen as a fuel. In order to guide the research into hydrogen storage, the U.S. Department of Energy (DOE) set gravimetric and volumetric storage targets for on-board hydrogen storage for 2010 (6 wt%, 45 g/L) and 2015 (9 wt%, 81 g/L) [32].

Current hydrogen storage techniques involve the use of high pressure tanks, cryogenic tanks, chemisorption, and physisorption. Pure tank-based hydrogen storage suffers from safety and economic issues [33]. The chemisorption approach allows the formation of chemical bonds between adsorbed hydrogen and the storage materials, leading to greater hydrogen storage density. However, the kinetics, reversibility and heat management still remain a problem [34]. Physisorption, on the other hand, is based on weak interactions (mainly van der Waals interactions) between the adsorbed hydrogen and the adsorbent, leading to fast kinetics, full reversibility, and manageable heat during hydrogen fueling. However, the promising data from physisorption-based hydrogen storage are all obtained at a cryogenic state (normally 77 K), and the adsorption becomes insignificant at ambient temperature.

In 2003, Rosi et al. reported the first MOF-based hydrogen storage study [35]. Subsequently, about 150 MOFs have been tested for their hydrogen uptake capacity [13], and several reviews focusing on this topic have appeared [13,36–41]. In order to avoid repetition, this section of the review will cover the most current literature and serve as an update to Ref. [13].

Hydrogen storage in MOFs is based on physisorption. It has been well established that under physisorption mode, the saturation hydrogen uptake at 77 K has a positive correlation with the surface area of the materials [13,38,40,42]. This is not surprising since increasing the surface area enhances the contact between hydrogen and the adsorbent resulting in an increased hydrogen uptake.

Compared to other porous materials, some MOFs have higher surface areas and subsequently higher hydrogen uptake capacity. One of the benchmarks is provided by the study on MOF-177, which has a BET surface area of 4500 m^2/g and an excess gravimetric hydrogen uptake of 7.5 wt% at 70 bar, 77 K [42,43]. However, when the temperature was raised to ambient temperature, the hydrogen uptake dropped significantly, as is the general case. The theoretical study from Bhatia and Myers demonstrated that an adsorption enthalpy change of 15.1 kJ/mol is needed for ambient temperature storage of hydrogen and delivery between 30 and 1.5 bar of pressure [44]. More importantly, the adsorption enthalpy change should be kept at the same level during the whole loading range. However, in current MOF-based hydrogen physisorption, the adsorption enthalpy change is only within the range of 4–10 kJ/mol [13], and the enthalpy drops dramatically as the adsorption amount increases. It has become clear that increasing the interaction between hydrogen and MOFs is the most important step towards practical usage of MOF-based hydrogen storage.

One way to increase the interaction between hydrogen and MOFs is to tailor the pore size in the MOF to maximize the potential overlap of the walls thereby allowing enhanced interaction between hydrogen and MOFs. Theoretical and experimental results support that the optimal pore size is around 6 Å, about twice the effective kinetic diameter of the hydrogen molecule [45]. A recent neutron diffraction study on rare earth MOFs indicated that the strong interaction between hydrogen and the optimized pore walls is comparable to the interaction between hydrogen and unsaturated metal centers, a point which will be discussed later [46]. Catenation, when two or more identical frameworks interpenetrate each other, could be used to generate MOFs with appropriate pore sizes for enhanced hydrogen uptake [36,47–50]. There is, however, a discrepancy between the theory and experimental results. The grand canonical Monte Carlo (GCMC) simulations done on the IRMOF (isoreticular metal-organic framework) series by Ryan et al. proposed that catenation can improve hydrogen uptake in IRMOFs at cryogenic temperatures and low pressures, but not at room temperature [51]. Based on these calculations, there is a temperature range at which catenation is beneficial for hydrogen uptake at low pressures. At higher pressures, however, the non-catenated IRMOFs adsorb more hydrogen due to a greater free volume (Fig. 4). At ambient temperature, catenation does not improve hydrogen uptake for the three IRMOFs studied. Using a template, Ma et al. have generated a pair of catenated and non-catenated MOFs, PCN-6 and PCN-6′ (Fig. 5) [49]. The low pressure and 77 K gas sorption results showed that catenation yields a 41% increase in Langmuir surface area and 133% enhancement in volumetric hydrogen uptake (29% in gravimetric). A further investigation of the effect of catenation on hydrogen uptake at higher pressure and ambient temperature shows promising results: 6.7 wt% at 77 K/50 bar (0.92 wt% at 298 K/50 bar) for PCN-6 *vs.* 4.0 wt% at 77 K/50 bar (0.40 wt% at 298 K/50 bar) for PCN-6′ [29]. Inelastic neutron scattering studies showed that the interaction between hydrogen and the organic linkers is stronger in catenated PCN-6 than in non-catenated PCN-6′ (Fig. 6). This may stem from a greater number of interactions from the atoms in the organic ligands, especially at high hydrogen loadings.

One advantage of using MOFs over other porous materials is that in some MOFs, unsaturated metal centers (UMCs) can be generated by the removal of the coordinated solvent molecules under vacuum [41]. The interaction between hydrogen and the UMCs is much higher than that with pure carbon materials, and the isosteric heat of adsorption can sometimes go as high as 12–13 kJ/mol [52,53], very close to the projected optimum 15.1 kJ/mol [44]. Lee et al. prepared isostructural MOFs with and without UMCs, and compared their hydrogen sorption capacities [54]. MOFs containing UMCs have higher hydrogen uptake both at low pressure (2.87 wt% *vs.* 2.07 wt% at 77 K/1 atm) and high pressure (5.22 wt% *vs.* 3.70 wt% at 77 K/50 bar) than MOFs with saturated metal centers. The higher

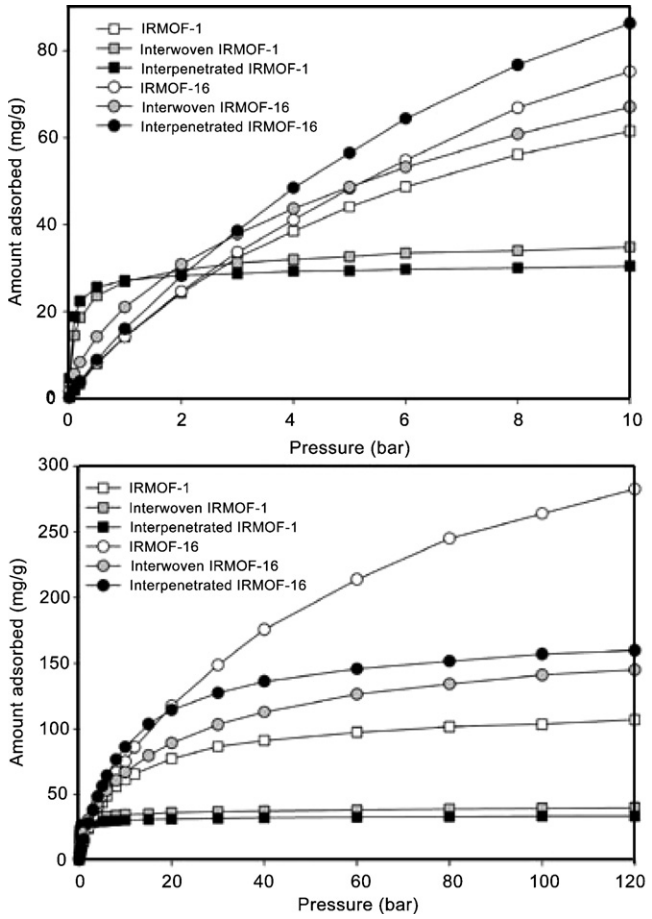

Fig. 4. Simulated hydrogen adsorption isotherms on IRMOFs. Reproduced with permission from Ref. [51].

hydrogen uptake capacity was attributed to the stronger interaction of hydrogen molecules with the UMCs of the MOF, and was supported by the higher zero-coverage isosteric heat of adsorption (11.60 kJ/mol *vs.* 7.24 kJ/mol).

It has been suggested that MOFs with cage-like polyhedral building units could be useful in the storage of small molecules, because adsorbed guests may remain kinetically trapped inside the cages [55]. By linking two isophthalate moieties with the dicopper paddlewheel motif, Wang et al. developed the “close-packing” strategy to generate MOFs with polyhedral cage structures and UMCs rationally aligned to interact directly with the guest inside the void [56]. The result was encouraging: the MOF with aligned UMCs (PCN-12) has much higher hydrogen uptake than the misaligned one (PCN-12′) (3.05 wt% *vs.* 2.40 wt%, 77 K/1 atm, Fig. 7). In the UMCs-aligned-MOF, the initially adsorbed hydrogen around the UMCs will point into the void, leading to higher potential overlap inside the void and higher affinity for the subsequent adsorbed hydrogen.

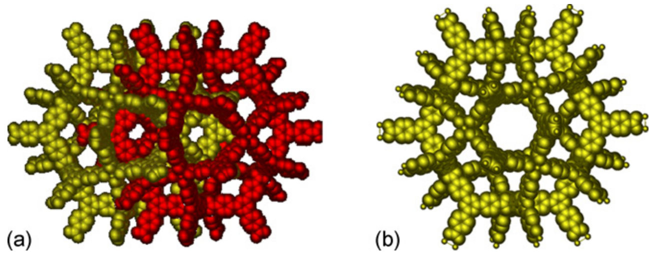

Fig. 5. (a) Catenated PCN-6. (b) Non-catenated PCN-6′. Reproduced with permission from Ref. [49].

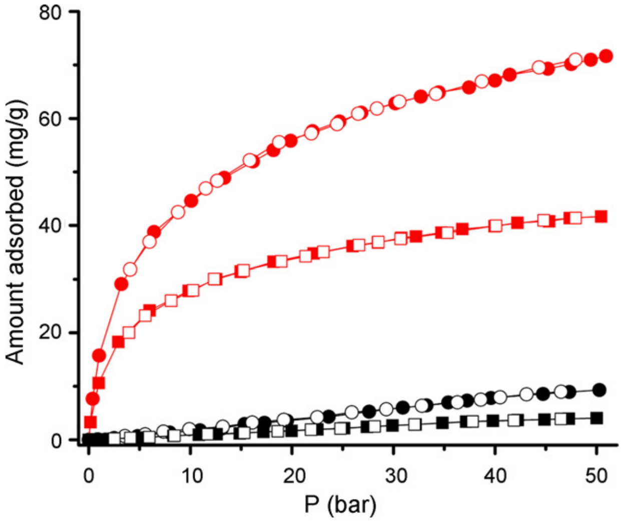

Fig. 6. Excess hydrogen sorption isotherms of PCN-6 and PCN-6′ at 77 K (red) and 298 K (black): circles, PCN-6; squares, PCN-6′; solid symbols, adsorption; open symbols, desorption. Reproduced with permission from Ref. [29]. (For interpretation of the references to color in this figure legend, the reader is referred to the web version of the article.)

Theoretical studies revealed that the binding energy between hydrogen and transition metals can be tuned from about 10 to 50 kJ mol^{-1} by using different transition metals in the MOF system [57]. This was partially confirmed by a recent experiment in which a series of isostructural MOFs were prepared from a vari-

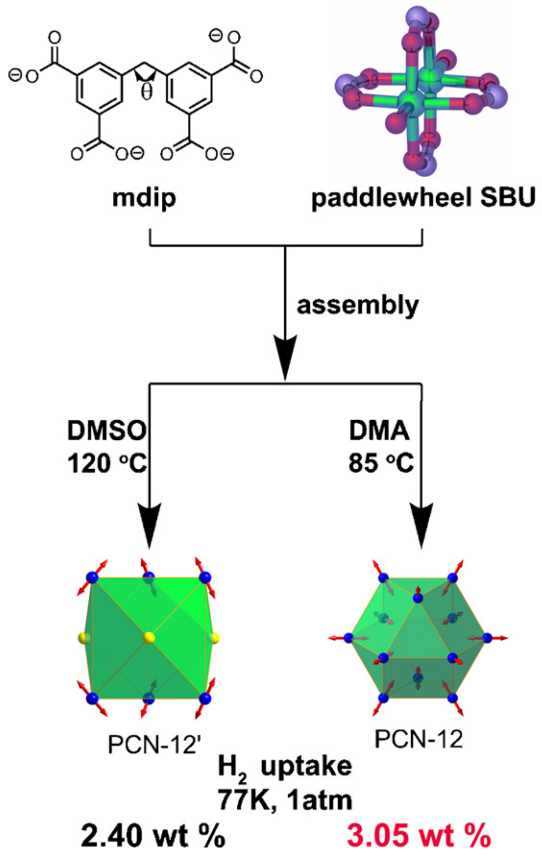

Fig. 7. The synthesis, UMCs alignment, and hydrogen uptake of two MOF polymorphs: PCN-12 and PCN-12′. Adapted from Ref. [56].

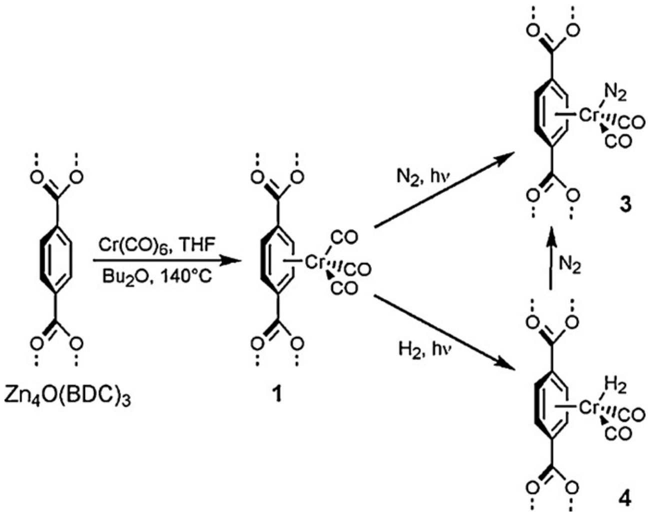

Fig. 8. Reaction of $Zn_4O(BDC)_3$ with $Cr(CO)_6$ to generate $Zn_4O[(BDC)Cr(CO)_3]_3$ (1), followed by photolysis under N_2 or H_2 to afford $Zn_4O[(BDC)Cr(CO)_2(N_2)]_3$ (3) and $Zn_4O[(BDC)Cr(CO)_2(H_2)]_3$ (4). Reproduced with permission from Ref. [65].

ety of metal ions (Mg, Mn, Co, Ni, Zn) [58]. The hydrogen sorption data showed that within this series the zinc MOF has the lowest heat of adsorption (~8.5 kJ/mol) while the nickel one has the highest (~12.9 kJ/mol), and the order of the heat of adsorption matches the Irving–Williams sequence [59] reasonably well. This confirmed previous calculations indicating that the major interaction between the UMCs and hydrogen molecules is Coulombic attractions [60]. Vitillo et al. studied the role of UMCs in hydrogen storage in MOFs of different natures and with different accessibilities of the UMCs [53]. Their results indicated that UMCs can increase the binding between hydrogen and MOFs, but their effect in the hydrogen uptake is almost completely hidden in the high pressure range where surface area and pore volume play primary roles. The efficiency of hydrogen storage by physisorption should increase as the surface density of UMCs is increased.

Many theoretical calculations support the idea that doping MOFs with metal ions could enhance the hydrogen uptake capacity [61–64]. This enhancement is proposed to originate from the strong interactions between hydrogen and the doped metal ions. However, this "ideal" metal ion geometry adopted in the calculated studies is very hard to achieve experimentally. Even though Kaye and Long developed a photosensitive doping method to embed chromium into MOFs (Fig. 8) [65], additional open coordination sites were very limited, and the gravimetric hydrogen uptake capacity was impaired due to the added mass. Mulfort and Hupp reported the doping of a catenated MOF with lithium ions by chemical reduction of the ligand with lithium metal [66]. The lithium-doped MOF exhibited a 75% increase in gravimetric hydrogen uptake (1.63 wt% *vs.* 0.93 wt% at 77 K/1 atm) and a higher heat of adsorption throughout the entire loading range (6–5 kJ/mol *vs.* 5.6–3.3 kJ/mol). The extreme enhancement of hydrogen binding (60 H_2 molecules per added Li^+) was attributed to the direct H_2/cation binding, as well as other factors such as framework displacement and/or enhanced strut polarizability.

A further study of the alkali metal cation effects on hydrogen uptake and binding in catenated MOFs was carried out using Li^+, Na^+, and K^+ [67]. The 77 K/1 atm gravimetric hydrogen uptake increase followed as $K^+ > Na^+ > Li^+$, while the isosteric heat of adsorption adopted the opposite trend (Fig. 9). Two observations cast doubt on the hydrogen–metal binding mechanism: (1) an extraordinarily large number of hydrogen molecules adsorbed per dopant cation; and (2) a much smaller isosteric heat of adsorption compared to the calculated result. More importantly, further doping with K^+ led to decreased hydrogen uptake. After careful examination of the nitrogen isotherms, the alkali metal cation effects were attributed to a molecular-adsorbate-driven displacement of interwoven networks, as well as the possible positioning of the dopant ions between the frameworks where they are not readily accessible to hydrogen. More recently it was reported that the metal doping increased the hydrogen uptake without a significant change of the heat of adsorption [68]. In order to rule out the effect of framework displacement in evaluating the doping ion's impact on the hydrogen uptake, Yang et al. prepared a Li^+-doped MOF by ion exchange within a non-catenated MOF [69]. Surprisingly, a 25% increase in gravimetric hydrogen uptake was observed while the Li^+-doped MOF displayed a lower isosteric heat for hydrogen adsorption than the original MOF. The increase in hydrogen uptake was attributed to the increase of BET surface area in the Li^+-doped MOF, and, additionally, there was no apparent interaction between adsorbed hydrogen and the exchanged Li^+.

Spillover techniques have been used to further advance hydrogen storage in MOFs. Hydrogen storage by spillover involves the split of diatomic hydrogen molecules into hydrogen atoms with the help of heavy transition metal (*e.g.* Pd) and the diffusion of the split hydrogen atoms onto the supportive framework (*e.g.* MOF) [70]. The initial results of MOF-based hydrogen storage by spillover demonstrated promising capacity and reversibility [71]. Proch et al. embedded Pt into MOF-177 via metal-organic chemical vapor deposition and tested the hydrogen uptake capacity at ambient

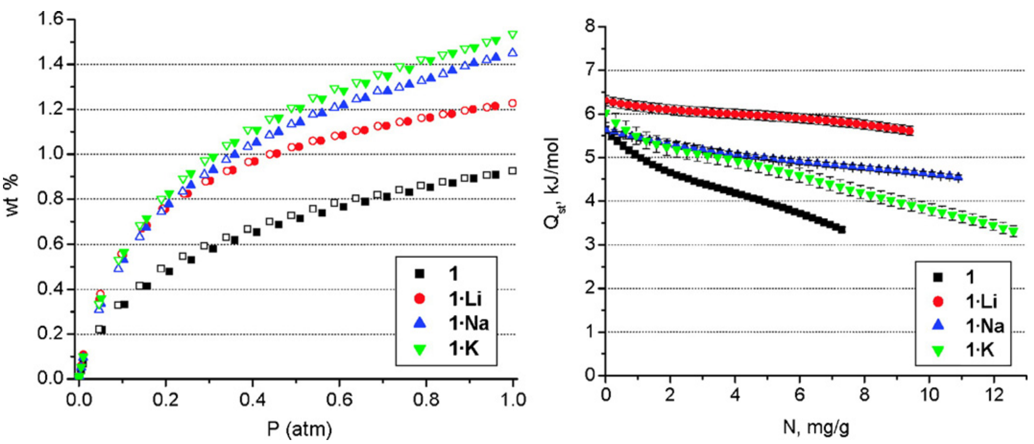

Fig. 9. Left: 77 K hydrogen isotherm for neutral MOF-1 and metal ion doped-MOF 1 M; Right: isosteric hydrogen heat of adsorption for 1 and 1 M. Reproduced with permission from Ref. [67].

temperature [72]. The first cycle showed an encouraging 2.5 wt% hydrogen uptake, but dropped to 0.5 wt% in consecutive cycles. The uptake loss was attributed to the formation of metal hydrides, which are not desorbed at ambient temperature.

Ionic MOFs are another proposed approach towards practical hydrogen storage in which the binding between hydrogen and MOFs can be enhanced by the attractive electrostatic interactions [73–75]. A calculation was performed by Kuc et al. in which the hydrogen molecule was placed in a fictitious linear $Na^+–H_2–Cl^-$ complex, where Na^+ and Cl^- were placed on opposite sides of hydrogen at a distance of 3.2 Å from the hydrogen center [76]. The dipole component at the center hydrogen molecule was calculated to be 0.73 (0.97) Debye using the NBO (Mulliken) charges; however, it is extremely difficult to introduce such a large charge separation in real MOF systems.

Despite the rapid advancement in MOF research, the DOE hydrogen storage target has yet to be reached with a pure MOF system. However, due to novel properties and well-defined structures, MOFs are still attracting much attention. For example, supercritical processing in the MOF activation step permits the opening of a gate of even higher surface area [77]. As reported from the high pressure hydrogen storage study done on IRMOF-1, the upper-limit hydrogen density based on the physisorption method would hardly go beyond the density of liquid hydrogen (70.8 g/L) [78]. It was further concluded that the development of a new method would be necessary to reach DOE's 2015 volumetric hydrogen storage target (81 g/L).

3.3. *Methane storage in MOFs*

Natural gas (NG) is another good candidate for on-board fuel. The main component of NG is methane (>95%), while the rest is a mixture of ethane, other hydrocarbons, nitrogen, and carbon dioxide [79]. Methane has a comparable gravimetric heat of combustion with gasoline (50.0 MJ/kg *vs.* 44.5 MJ/kg) [31], but it suffers from the lack of effective storage. Liquefied natural gas (LNG) can provide about 72% of the volumetric energy density of gasoline yet requires cryogenic conditions (112 K). Compressed natural gas (CNG) can offer about 26% of the volumetric energy density of gasoline but operates at pressures about 200 bar for compression [79]. Adsorbed natural gas (ANG) provides another storage method in which NG is adsorbed on a porous adsorbent, and the volumetric storage energy density for ANG (at 500 psig) has been reported to be up to 80% of that of CNG (at 3000 psig) [79].

Unlike for hydrogen, the heat of adsorption for methane (about 20 kJ/mol) is already within the ideal scope for practical usage. DOE has set a methane storage target: 180 v/v at ambient temperature and pressure no more than 35 bar [80]. Some of the carbon materials have already reached this target [79], but they have limited packing density. Thus, the focus has been on increasing the surface area of the porous sorbent.

In 1997, Kondo et al. reported the first methane sorption study using MOFs [81]. Table 1 summarizes the surface area, porosity and methane uptake data for selected MOFs. The breakthrough result obtained by Ma et al. showed that the methane uptake in a MOF can exceed the DOE target [82].

One point of concern is that uptake data calculations are based on the MOFs' crystallographic density, which is higher than the packing density due to the void generated by particle packing [83]. More methane uptake data needs to be calculated from the MOFs real packing density from MOFs in order to evaluate the potential of MOFs in methane storage.

4. Selective gas adsorption in MOFs

4.1. *Introduction*

With the ever-increasing demand for cheaper and more environmentally friendly industrial applications, new means for selective gas adsorption and separation are being examined. Currently, industrial methods for selective gas adsorption rely heavily on cryogenic as well as membrane- and adsorption-based techniques. In adsorption-based separation, commonly used adsorbents include zeolites, molecular sieves, carbon nanotubes, aluminosilicates, and silica gel [89–94]. A review of the individual properties and usages in industry of these materials is beyond the scope of this review. However, all materials for selective gas adsorption are chosen based on two main criteria: (1) the adsorption capacity of the adsorbent; and (2) the selectivity of the adsorbent for an adsorbate [2]. These properties are dictated by the chemical composition and structure of the adsorbent, as well as the equilibrium pressure and temperature during the adsorption. MOFs are very promising candidates for selective gas adsorption, which can lead to gas separation. In particular, mesh-adjustable molecular sieve (MAMS) [95] is such a new type of MOFs that stands out due to its remarkable selectivity and tunable properties. A complete review of selective gas adsorption and separation in metal-organic frameworks can be found in Ref. [2].

Table 1
Surface area, porosity, and methane uptake data for selected MOFs.

Material[a]	Surface area ($m^2 g^{-1}$)		Pore volume ($cm^3 g^{-1}$)	Density[b] ($g cm^{-3}$)	Ambient temperature CH_4 uptake		ΔH_{ads} ($kJ mol^{-1}$)	Ref.
	BET	Langmuir			wt%	v/v		
$Co_2(4,4'\text{-bipy})_3(NO_3)_4$				1.36	3.6 (30.4 bar)	71		[81]
$Cu_2(pzdc)_2(pyz)$				1.75	1.3 (31.4 bar)	32		[84]
$Cu_2(pzdc)_2(4,4'\text{-bipy})$					3.9 (31.4 bar)			[84]
$Cu_2(pzdc)_2(pia)$					4.4 (31.4 bar)			[84]
$CuSiF_6(4,4'\text{-bipy})_2$				0.86	9.4 (36.5 bar)	124		[85]
$Zn_4O(R_6\text{-bdc})_3$ IRMOF-6		2630	0.60	0.65	14.7 (36.5 bar)	155		[86]
MIL-53(Al) Al(OH)(bdc)	1100	1590	0.59	0.98	10.2 (35 bar)	155	17	[87]
MIL-53(Cr) Cr(OH)(bdc)	1100	1500	0.56	1.04	10.2 (35 bar)	165	17	[87]
PCN-14 $Cu_2(adip)$	1753		0.87	0.83	16.0 (35 bar)	220	30	[82]
PCN-11 $Cu_2(sbtc)$	1931	2442	0.91	0.75	14.1 (35 bar)	171	14.6	[88]
HKUST-1 $Cu_3(btc)_2$	1502	2214	0.76	0.88	15.7(150 bar)	228		[83]
$Zn_2(bdc)_2dabco$	1448	2104	0.75	0.87	14.3 (75 bar)	202		[83]
MIL-101 $Cr_3FO(bdc)_3$	2693	4492	1.303	0.31	14.2 (125 bar)	72		[83]

[a] 4,4′-bpy = 4,4′-bipyridine, pzdc = pyrazine-2,3-dicarboxylate, pyz = pyrazine, pia = *N*-(pyridin-4-yl)isonicotinamide, R_6-bdc = 1,2-dihydrocyclobutabenzene-3,6-dicarboxylate, dbc = benzenedicarboxylate, adip = 5,5′-(9,10-anthracenediyl)di-isophthalate, abtc = azobenzene-3,3′,5,5′-tetracarboxylate, sbtc = trans-stilbene-3,3′,5,5′-tetracarboxylate, btc = benzene-1,3,5-tricarboxylate, dabco = 1,4-diazabicyclo[2.2.2]octane.

[b] Calculated from single crystal structure without guest molecule and labile ligand binding.

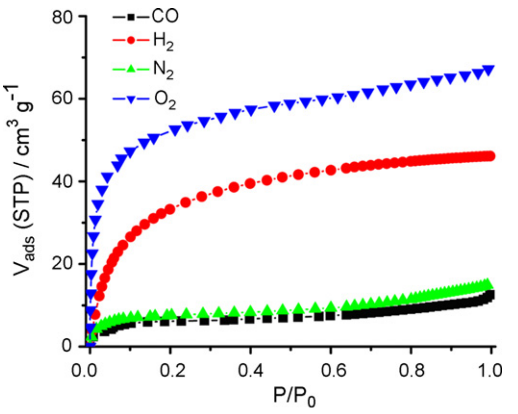

Fig. 10. Hydrogen, oxygen, nitrogen, and carbon monoxide adsorption isotherms of PCN-13 at 77 K. Reproduced with permission from Ref. [96].

4.2. Selective gas adsorption in MOFs

The principal mechanisms based on which selective gas adsorption is achieved in MOFs are adsorbate–surface interactions and size-exclusion (molecular sieving effect). The former involves the chemical and/or physical interaction between the adsorbent and the adsorbate while the latter depends on the dimension and shape of the framework pores. It is important to keep in mind that the two effects are capable of working independently as well as cooperatively.

4.2.1. Selective gas adsorption of O_2 over N_2 based on size-exclusion in rigid MOFs

Selective gas adsorption based on size-exclusion principle has been successfully demonstrated with several MOFs. PCN-13 ($Zn_4O(H_2O)_3(C_{16}H_8O_4)_3 \cdot 2DMF$) contains a square hydrophobic channel of 3.5 Å × 3.5 Å and has a pore volume of 0.3 cm^3/g [96]. The larger size of the N_2 molecule (kinetic diameter of 3.64 Å) as opposed to the O_2 molecule (kinetic diameter of 3.46 Å) completely prevents N_2 from entering the aperture while allowing O_2 to pass through the pore as shown in Fig. 10. Likewise, $Mg_3(ndc)_3$, with its pore opening of approximately 3.46–3.64 Å, demonstrates almost no N_2 uptake at 77 K and 880 Torr whereas approximately 3.5 mmol/g of O_2 is adsorbed [97]. PCN-17 ($Yb_4(\mu_4\text{-}H_2O)(C_{24}H_{12}N_3O_6)_{8/3}(SO_4)_2 \cdot 3H_2O \cdot 10DMSO$), with its large cages connected by small apertures, is able to selectively adsorb over ten times as much O_2 as N_2 [98].

4.2.2. Selective gas adsorption based on size-exclusion in dynamic MOFs

The cases in the foregoing discussion involve MOFs that are classified as rigid and do not display any obvious flexible behavior. Dynamic, or flexible MOFs exist and their applications depend not only on the size of the aperture, but also on adsorption conditions (pore sizes vary with pressure/temperature adjustment and/or are controlled by host–guest induced gate opening) [2]. Nevertheless, the adsorption selectivity of O_2 over N_2, based mainly on size-exclusion in dynamic MOFs, has also been observed. $Ni_2(cyclam)_2(mtb)$ can selectively adsorb O_2 because its interpenetrated network results in narrow channels that are only large enough for O_2 molecules to pass through [99].

4.2.3. Selective gas adsorption based on adsorbate–surface interactions in rigid MOFs

Adsorbate–surface interactions also play a very important role in the selective gas adsorption of O_2 over N_2. For example, the pore walls of the rigid MOF Cu(bdt) contain unsaturated metal coordination sites, leading to high affinity for O_2. This MOF can adsorb 14 mmol of O_2 but only 3 mmol of N_2 [100].

4.2.4. Selective gas adsorption based on adsorbate–surface interactions in dynamic MOFs

The adsorbent–guest interactions in dynamic MOFs have also demonstrated adsorption selectivity of O_2 over N_2 [99,101–103]. Depending on the interaction between the adsorbate and the adsorbent, pore expansion or constriction also occurs. This is known as the gate-opening process [2]. Characteristic gate-opening selective adsorption of O_2 over N_2 has been observed in Cd(bpndc)(4,4′-bpy), in which approximately 150 mL/g of O_2 was adsorbed with almost no N_2 uptake [103]. This significant difference in gas uptakes was attributed to the interaction of the O_2 molecules with the framework, which is stronger than that of N_2. Similar results have been shown with $Cu(dhbc)_2(4,4'\text{-bpy})$ and $Cu(bdc)(4,4'\text{-bpy})_{0.5}$ but with less uptake of O_2 [101,102].

4.3. Useful gas separations in MOFs

The separation of alkane isomers from natural gas is of primary concern for industrial applications. It has been demonstrated that MOF-508 may be utilized to separate such alkanes using gas chromatographic techniques [104]. The 3D pillared layer provides the necessary framework to selectively separate linear and branched alkanes by adsorbing the linear ones while allowing the branched alkanes to pass because of the difference in van der Waals interactions between the isomers and the frameworks' pores [105]. Additionally, this MOF proved effective in separating natural gas mixtures through gas chromatography.

Recently, MOFs have been incorporated into thin-film materials to aid in gas separation. The copper net supported $Cu_3(btc)_2$ MOF thin film developed by Guo et al. demonstrated the successful separation of H_2 from H_2/N_2, H_2/CO_2, and H_2/CH_4 mixtures [106]. This MOF demonstrated excellent permeation selectivity for H_2 and possessed separation factors much higher than traditional zeolites (Fig. 11). The recyclability of this MOF further enhances its potential for application in H_2 separation and purification.

Recently, Couck et al. demonstrated the successful separation of CO_2 and CH_4 gases using amino-functionalized MIL-53(Al) [107]. Because CO_2 possesses a quadrupole moment, the CO_2 molecules have a high affinity for the amino groups. Breakthrough experiments demonstrated that the weakly adsorbed CH_4 is able to pass through a MOF-packed column while CO_2 is adsorbed. Thus, efficient separation of the two gases can be performed at ambient conditions, as shown in Fig. 12.

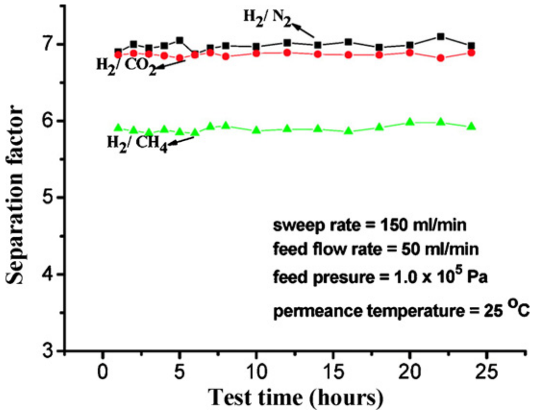

Fig. 11. The separation factors for various H_2 gas mixtures by copper net supported $Cu_3(btc)_2$ MOF thin film. Reproduced with permission from Ref. [106].

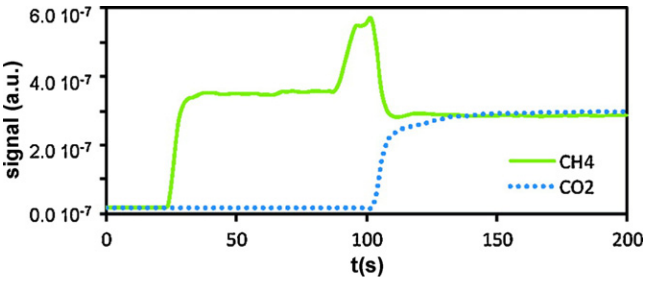

Fig. 12. Separation of CO_2 and CH_4 gas mixtures using amino-MIL-53(Al). Reproduced with permission from Ref. [107].

4.4. *MAMS in selective gas adsorption*

One of the most promising materials for selective gas adsorption is the MOF-based mesh-adjustable molecular sieve [95]. MAMS are very useful when attempting to separate gases in which the difference in size is very small. Unlike in more rigid systems, the pore sizes in MAMS can be tuned across a wide array by simply adjusting the temperature (Fig. 13). Such a material has recently been reported by Ma et al. as MAMS-1, a layered structure with hydrophilic channels and hydrophobic chambers interconnected through a size-adjustable gate [95]. In MAMS-1, the hydrophobic chambers are the site of gas storage, yet the gas must first pass through the hydrophilic channels. Between the hydrophilic channels and the hydrophobic chambers lie two bbdc ligands that serve as the gate that can be opened or closed with an increase or decrease in temperature, respectively. By simply varying the temperature between 60 and 300 K, the gate size of MAMS-1 can be adjusted anywhere from 2.9 to 5.0 Å. Thus, fractional adsorption may be attained on MAMS-1 for separation of virtually any multi-component gas so long as the target molecule's kinetic diameter falls within this range. Industry-relevant experiments have been carried out on MAMS-1 and have demonstrated selective adsorption of H_2 over CO_2, O_2, and N_2 at 77 K; O_2 over CO and N_2 at 87 K; N_2 over CO_2 and CH_4 at 113 K; CH_4 over C_2H_4 at 143 K; C_2H_4 over C_3H_6 at 196 K; C_3H_6 over *iso*-C_4H_{10} at 241 K [95]. In addition, the MOFs $Mn(HCOO)_2$ and Cu(etz) also exhibit temperature-dependent gate-opening behavior [108,109].

Isostructural MAMSs (MAMS-2, MAMS-3, and MAMS-4, prepared with metal centers of Zn, Co, and Cu, respectively) also display temperature-dependant molecular sieving effects [110]. Like MAMS-1, a linear relationship exists between temperature and mesh size, with the new MAMSs mesh size existing anywhere from 2.9 to 4.6 Å when the temperature is adjusted from 77 to 273 K. As temperature increases, the van der Waals interactions between the *tert*-butyl groups of the ligands of the framework decrease, thus allowing larger molecules to pass through the frameworks' gate. This selectivity provided selective adsorption of O_2, $N_{2,}$ CO, ethylene, butane, and, theoretically, any gas that has a kinetic diameter between 2.9 and 4.6 Å.

5. Catalysis in MOFS

5.1. *Introduction*

As porous materials, MOFs may prove to be very useful in catalysis. Theoretically, the pores of MOFs can be tailored in a systematic way allowing optimization for specific catalytic applications. Besides the high metal content of MOFs, one of their greatest advantages is that the active sites are rarely different because of the highly crystalline nature of the material. Although catalysis is one of the most promising applications of such materials, only a few examples have been reported to date. In these MOFs, size- and shape-selective catalytic applications depend on porosity and the presence of catalytically active transition-metal centers.

5.2. *Catalysis in MOFs with active metal sites*

Zou et al. have prepared a 3D functional MOF by using a discrete metal–organic cubic building block $[Ni_8L_{12}]^{20-}$ (H_3L = 4,5-imidazoledicarboxylic acid) bridged by alkali-metal ions (Na^+) [111]. This MOF exhibited stable catalytic activity for the oxidation of CO to CO_2. Fig. 14b shows the rate of CO oxidation, R_{QMS}, obtained by quadrupole mass spectroscopy in comparison with those for Ni–Y zeolite and nickel oxide (NiO).

Gándara et al. obtained a new In(III) MOF composed of thick layers containing square-shaped channels (Fig. 14a) [112]. The channels are empty in In(OH)L and filled with pyridine in $[In(OH)L]\cdot xPy$ (L = 4,4′-(hexafluoroisopropylidene)bis(benzoic acid)). This microporous, thermally stable compound has been proven to be an efficient heterogeneous catalyst for acetalization of aldehydes (Fig. 14b). The difference in catalytic activity between compounds with empty or filled channels demonstrates that catalysis does indeed take place inside the pores.

5.3. *Catalysis in MOFs doped with metal catalysts*

Recently, Eddaoudi and co-workers have demonstrated the utilization of In-HImDC-based *rho*-ZMOF (Fig. 15a) as a host for large catalytically active molecules, specifically metalloporphyrins, and its effect on the enhancement of catalytic activity [113]. To produce a versatile platform, they encapsulated the free-base porphyrin which was readily metallated and post-synthetically modified by various transition metal ions to produce a wide range of encapsulated metalloporphyrins. Hydrocarbon oxidation was performed in the presence of Mn-RTMPyP (5,10,15,20-tetrakis(1-methyl-4-pyridinio)porphyrin tetra(*p*-toluenesulfonate encapsulated in *rho*-ZMOF) to assess catalytic activity for cyclohexane oxidation (Fig. 15b).

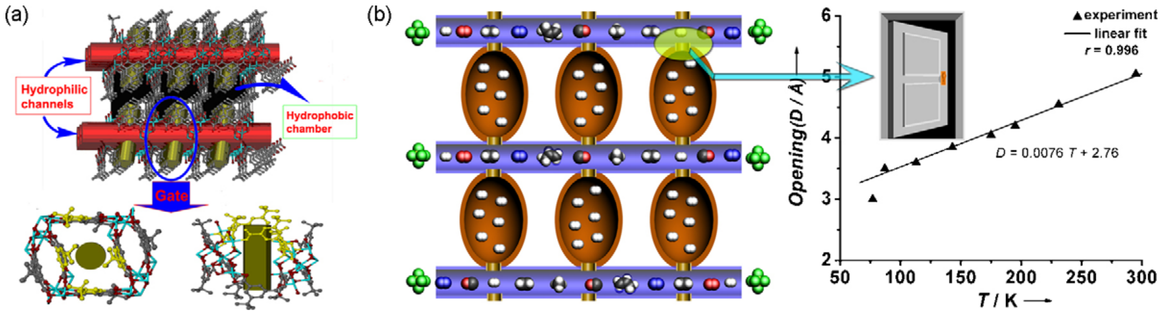

Fig. 13. The structure of MAMS-1 and the pore opening dependence on temperature. Reproduced with permission from Ref. [2].

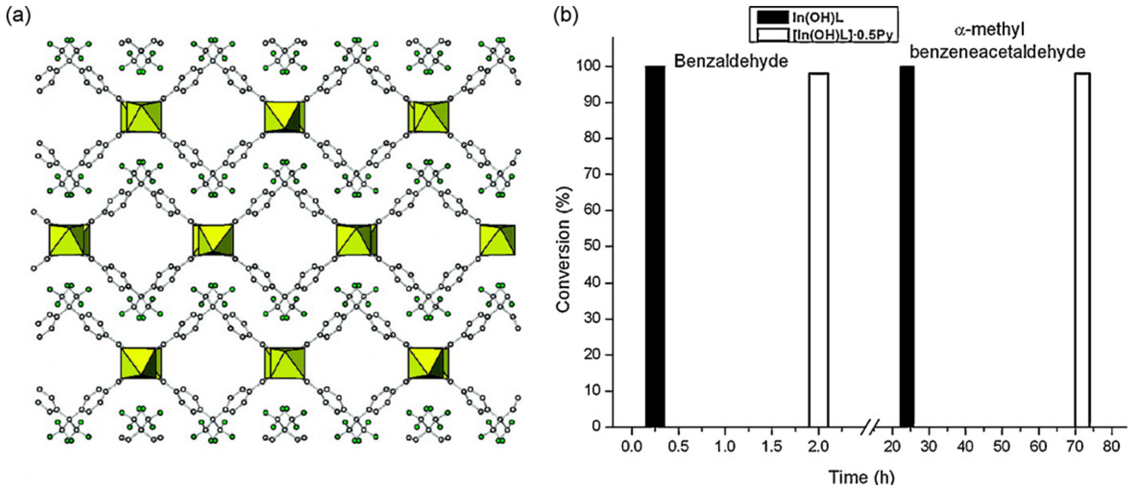

Fig. 14. (a) Polyhedral representation of the structure. (b) Acetalization catalyzed by [In(OH)L]·0.5Py (white columns) and [In(OH)L] (black columns). Reproduced with permission from Ref. [112].

The embedding of Ru nanoparticles in the otherwise unchanged metal-organic framework MOF-5 has been investigated by Schröder et al. (Fig. 16) [114]. After the inclusion of Ru to form [Ru(cod)(cot)]$_{3.5}$@MOF-5, hydrogenolysis formed Ru nanoparticles inside the cavities and lead to the material Ru@MOF-5. Preliminary results for alcohol oxidation with Ru@MOF-5 revealed limited catalytic applications of the water-sensitive MOF-5 host material.

5.4. Catalysis in post-synthesized MOFs

Hwang et al. found that the presence of chromium(III) coordinatively unsaturated metal sites (CUSs) in chromium(III) terephthalate MIL-101 can provide an intrinsic chelating property with electron-rich functional groups that leads to the formation of the thermally stable amine species grafted to the surface (Fig. 17) [115]. This feature offers a powerful way to selectively functionalize the unsaturated sites in MIL-101. It was demonstrated that ethylenediamine and diethylenetriamine can be used as new grafting agents to produce the amine-grafted MIL-101, which exhibit remarkably high activities in the Knoevenagel condensation. Additionally, palladium loaded APS-MIL-101 and ED-MIL-101 have high activities during the Heck reaction (393 K), a powerful reaction used to couple alkenes with organic moieties.

Recently Ingleson et al. reported the rational, post-synthetic modification of a series of MOFs, M(asp)L$_{0.5}$ (M = Ni^{2+} or Cu^{2+}, asp = L-aspartate or D-aspartate, L = bipy or bpe) (Fig. 18) [116]. The protonated frameworks needed to conduct acid-catalyzed reactions were generated by simply treating the porous, homochiral MOFs with HCl in diethyl ether. Containment within the MOF pore wall is crucial and no homogeneous analogues are known.

5.5. Selective catalysis in MOFs

Kitagawa and co-workers successfully synthesized a 3D porous coordination polymer (PCP) functionalized with amide groups, ([Cd(4-btapa)$_2$(NO$_3$)$_2$]·6H$_2$O·2DMF)$_n$, from the reaction between Cd(NO$_3$)$_2$·4H$_2$O and a three connector-type amide ligand (4-btapa) [117]. The amide groups are ordered uniformly on the channel surfaces (Fig. 19a) and facilitate the selective accommodation and activation of guests within the channels. Knoevenagel condensation reactions of benzaldehyde with active methylene compounds (*e.g.* malononitrile, ethyl cyanoacetate, and cyano-acetic acid *tert*-butyl ester) were conducted (Fig. 19b). While malononitrile proved to be a good substrate (98% conversion), the other substrates produced negligible results implicating a relationship between the size of the reactants and the pore window of the host.

The catalytic activity of the sodalite-type compound Mn$_3$[(Mn$_4$Cl)$_3$(BTT)$_8$(CH$_3$OH)$_{10}$]$_2$ has been investigated by Long et al. The compound is a thermally stable microporous solid exhibiting a cubic network of 7 and 10 Å pores that affords a BET surface area of 2100 m^2 g^{-1} [118]. The surface contains exposed Mn^{2+} ions that serve as Lewis acids (Fig. 20). Indeed, this compound catalyzes the cyanosilylation of aromatic aldehydes and ketones, as well as the more demanding Mukaiyama-aldol reaction. Moreover, in each

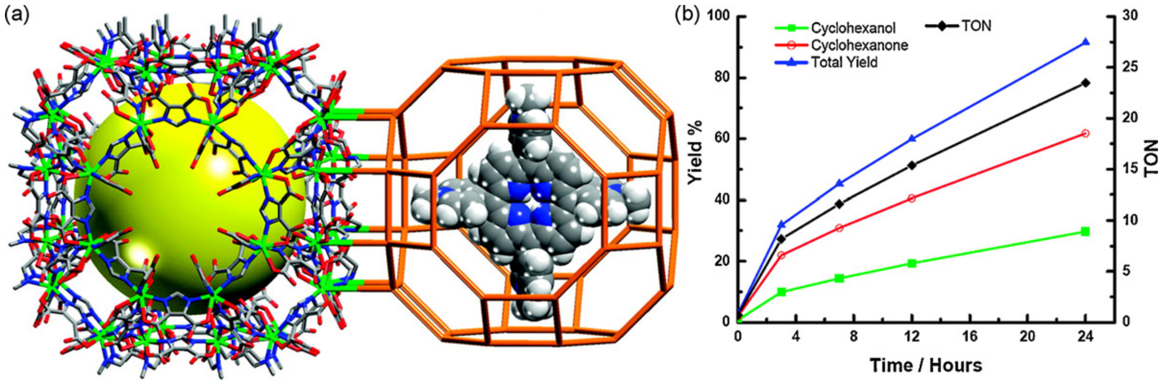

Fig. 15. (a) Crystal structure of *rho*-ZMOF (left) and schematic presentation of [H$_2$TMPyP]$^{4+}$ porphyrin ring enclosed in *rho*-ZMOF R-cage (right, drawn to scale). (b) Cyclohexane catalytic oxidation using Mn-RTMPyP as a catalyst at 65 °C. Reproduced with permission from Ref. [113].

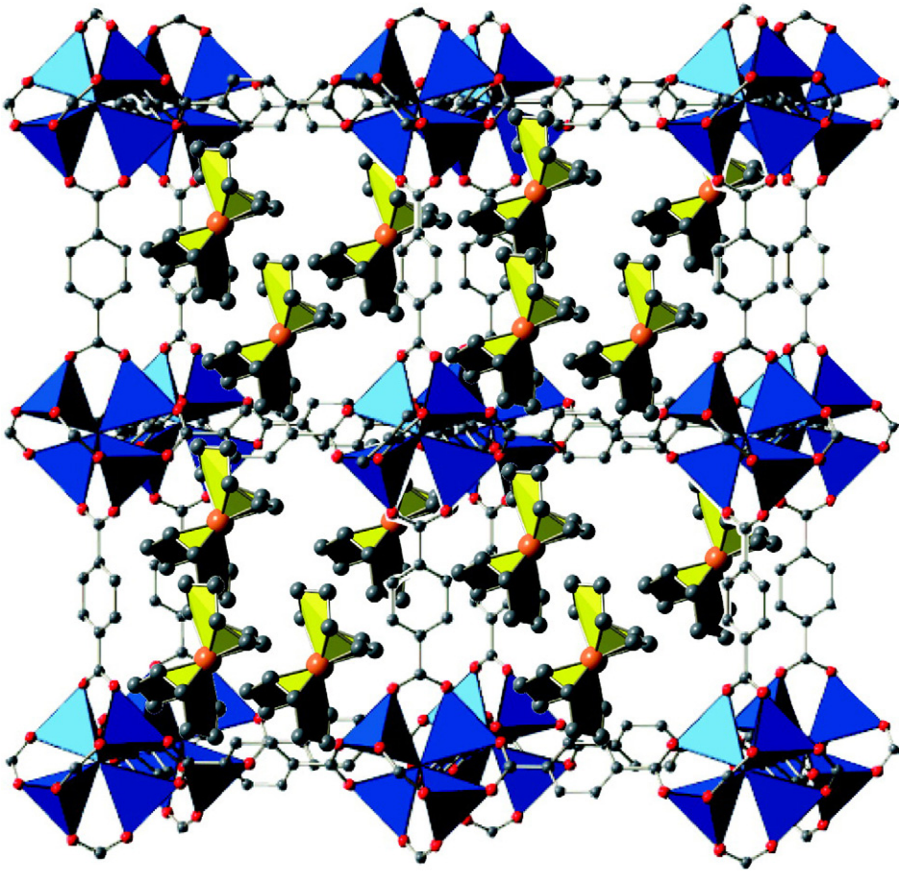

Fig. 16. Model of the inclusion compound $[Ru(cod)(cot)]_{3.5}$@MOF-5. Reproduced with permission from Ref. [114].

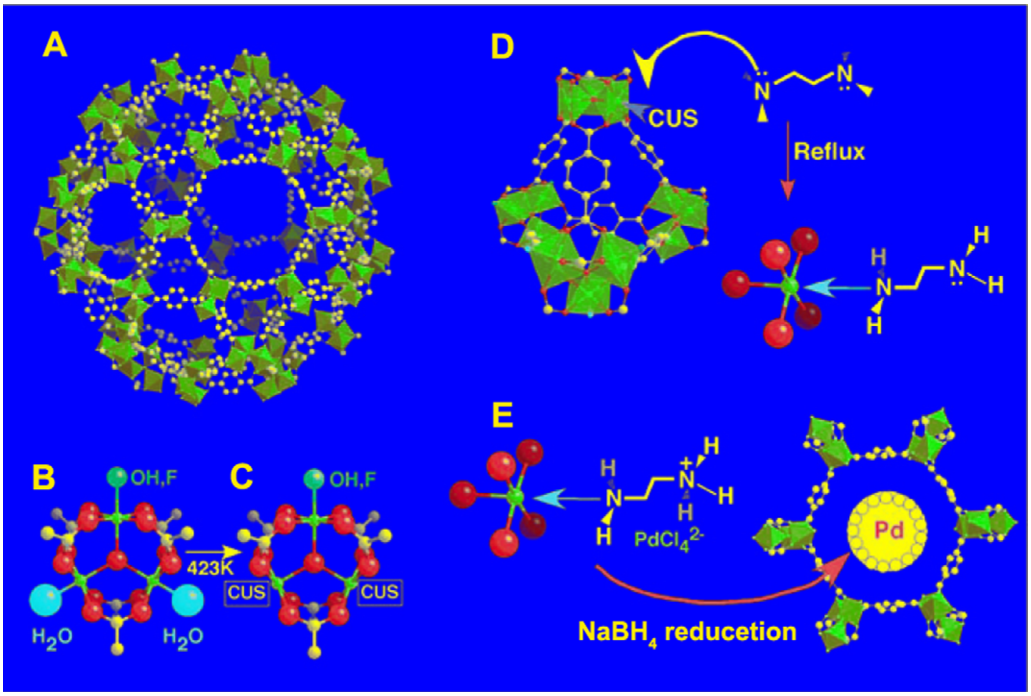

Fig. 17. Site-selective functionalization of MIL-101 with unsaturated metal sites: (A) perspective view of the mesoporous cage of MIL-101 with hexagonal windows; (B, C) evolution of coordinatively unsaturated sites from chromium trimers in mesoporous cages of MIL-101 after vacuum treatment at 423 K for 12 h; (D) surface functionalization of the dehydrated MIL-101 through selective grafting of amine molecules onto coordinatively unsaturated sites; (E) selective encapsulation of noble metals in the amine-grafted MIL-101 via a three-step process. Adapted from Ref. [115].

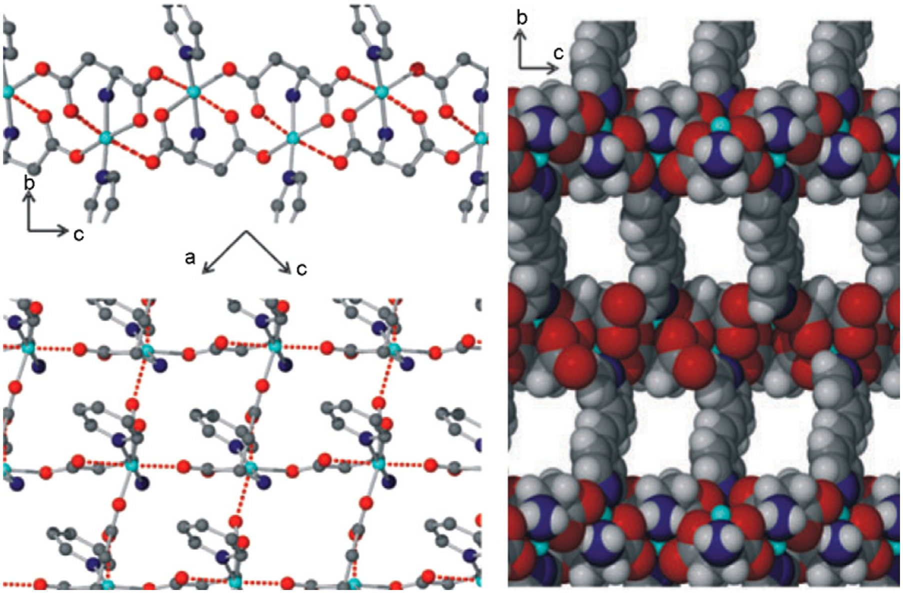

Fig. 18. Left, Cu(asp) 2D layer dashed red lines emphasise Jahn–Teller elongated Cu–O bonds. Right, cross-sectional view down the *a* axis (solvent removed for clarity) displaying the 1D porous channels between chiral Cu(asp) layers. Reproduced with permission from Ref. [116]. (For interpretation of the references to color in this figure legend, the reader is referred to the web version of the article.)

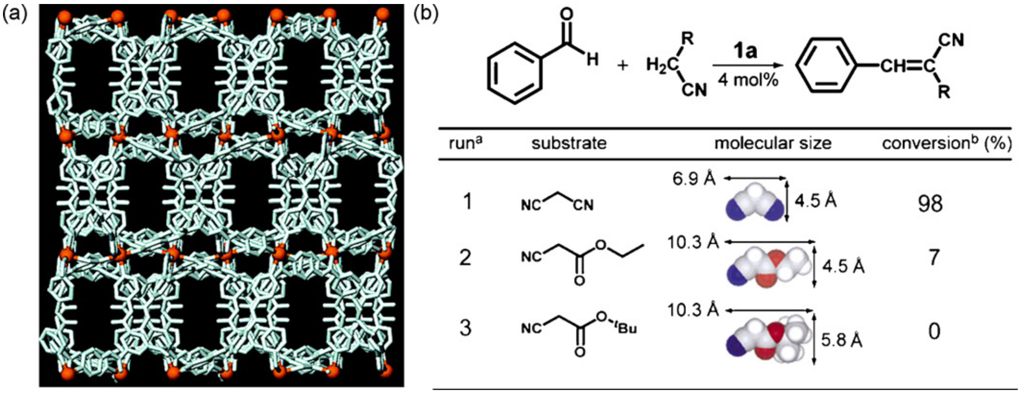

run^a	substrate	molecular size	conversion^b (%)
1		6.9 Å × 4.5 Å	98
2		10.3 Å × 4.5 Å	7
3		10.3 Å × 5.8 Å	0

Fig. 19. (a) Crystal structure to form another type of zigzag channels with dimensions of 3.3 Å × 3.6 Å. (b) Knoevenagel condensation reaction of benzaldehyde with substrates. Reproduced with permission from Ref. [117].

case, a pronounced size-selectivity effect consistent with the pore dimensions is observed.

5.6. *Catalysis in chiral MOFs*

In 2000, Seo et al. [119] reported the synthesis of a homochiral metal-organic porous material, $[Zn_3(\mu_3\text{-}O)(L)_6]\cdot 2H_3O\cdot 12H_2O$ (referred to as D-POST-1, L = D-tartaric acid), which uses enantiopure metal-organic clusters as secondary building blocks (Fig. 21a). The presence of the pyridyl groups exposed in the channels also provides POST-1 with unique opportunities in catalysis. The catalytic transesterification of ethanol occurred in 77% yield with POST-1 (Fig. 21b). The transesterification with bulkier alcohols such as isobutanol, neopentanol and 3,3,3-triphenyl-1-propanol using transesterification occurred at a much slower or even negligible rate under otherwise identical reaction conditions (Fig. 21c).

Wu and Lin synthesized a homochiral porous MOF, $[Cd_3L_4(NO_3)_6]\cdot 7MeOH\cdot 5H_2O$ (L = (R)-6,6′-dichloro-2,2′-dihydroxy-1,1′-binaphthyl-4,4′-bipyridine), by slow diffusion of diethyl ether into a mixture of $Cd(NO_3)_2\cdot 4H_2O$ and (R)-6,6′-dichloro-2,2′-dihydroxy-1,1′-binaphthyl-4,4′-bipyridine in DMF/$CHCl_3$/MeOH at room temperature (Fig. 22) [120]. Treatment of this compound with excess $Ti(O^iPr)_4$ in toluene led to an active catalyst for the addition of diethylzinc to aromatic aldehydes to afford chiral secondary alcohols upon hydrolytic workup. Chiral secondary alcohols were generated by this MOF in very high yields and enantioselectivities. For example, the addition of diethylzinc to 1-naphthaldehyde was catalyzed to afford (R)-1-(1-naphthyl)-propanol with complete conversion and 90.0% ee.

5.7. *Future research*

Future research should be dedicated to elucidate whether the metal centers, the ligands, particle size, or some combination of these can engender MOFs with unusual catalytic properties. More work is needed to determine if MOFs can compete with well-known heterogeneous industrial catalysts.

6. Magnetic properties of MOFs

6.1. *Introduction*

Magnets are very important materials with an ever-increasing number of uses. Thus, an important goal of the research of mag-

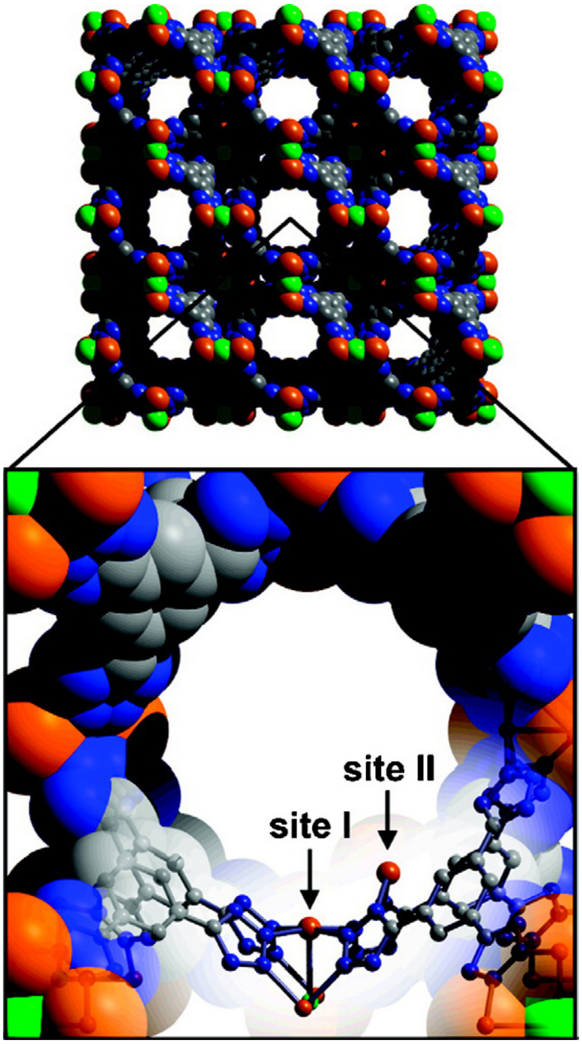

Fig. 20. A portion of the crystal structure showing the two different types of Mn^{II} sites exposed within its three-dimensional pore system of 10 Å wide channels. Site I is five-coordinate, while site II is only two-coordinate; the separation between them is 3.420(8) Å. Reproduced with permission from Ref. [118].

netic materials is the improvement of the properties of magnets as well as exploring new functions, in particular in combination with other useful phenomena [121]. The magnetic properties such as ferromagnetism, antiferromagnetism, and ferrimagnetism of polymetallic systems derive from the cooperative exchange interactions between the paramagnetic metal ions or organic radicals through diamagnetic bridging entities. Therefore, their magnetic behaviors depend on the intrinsic nature of both the metal and the organic ligand as well as the particular level of organization created by the metal–ligand coordination interaction. As a result, in pursuing the magnetism of MOFs, the ligand design is crucial both to organize the paramagnetic metal ions in a desired topology and to efficiently transmit exchange interactions between the metal ions in a controlled manner. The formation of a bulk material with non-zero spin requires a framework that allows for parallel coupling of the spins of neighboring paramagnetic spin carriers or antiparallel coupling of unequal spins. Canted spin orientations may also result. It should be pointed out that there is always a tendency for antiparallel coupling of spins because the state of low-spin multiplicity is often more stable than the state of high-spin multiplicity [122].

Magnetic studies of MOFs are embedded in the area of molecular magnets and the design of low-dimensional magnetic materials, magnetic sensors, and multifunctional materials. Indeed, closed-shell organic ligands that are typically used in MOFs mostly give rise to only weak magnetic interactions. In order to achieve a strong coupling between the metal centers, short oxo, cyano, or azido bridges are needed [123–125]. Alternatively, polymeric metal cyanide compounds are frequently encountered in magnetic investigations but fall outside the scope of this review. Furthermore, the porosity of MOFs provides additional interesting phenomena in regards to magnetic properties. The use of chemical coordination or crystal engineering techniques allows for the systematic design of MOFs with adjustable magnetic properties. Because the magnetic properties of MOFs have been recently reviewed [122,126–128], this section will give only a brief enumeration of recent results in the investigations of magnetic MOFs.

6.2. *Magnetic properties of MOFs*

6.2.1. *Ferromagnetic properties*

Ferromagnetism requires a structure that allows for parallel coupling of the spins. There are numerous reports about the magnetic properties of MOFs; however, literature on ferromagnetic MOFs is still limited. Biswas et al. [129] reported a magnetic MOF material, $\{[Cu_2(pic)_3(H_2O)]ClO_4\}_n$ (pic = 2-picolinate), which is constructed by “fish backbone” chains through *syn-anti* carboxylate groups. These chains are linked to one another by *syn-anti* carboxylate groups to give rise to a rectangular grid-like 2D net as shown in Fig. 23a. The ClO_4^- anions are located between these 2D cationic sheets. Magnetic susceptibility measurements revealed the presence of weak ferromagnetic coupling for this MOF that has been fitted with a suitable model (Fig. 23b).

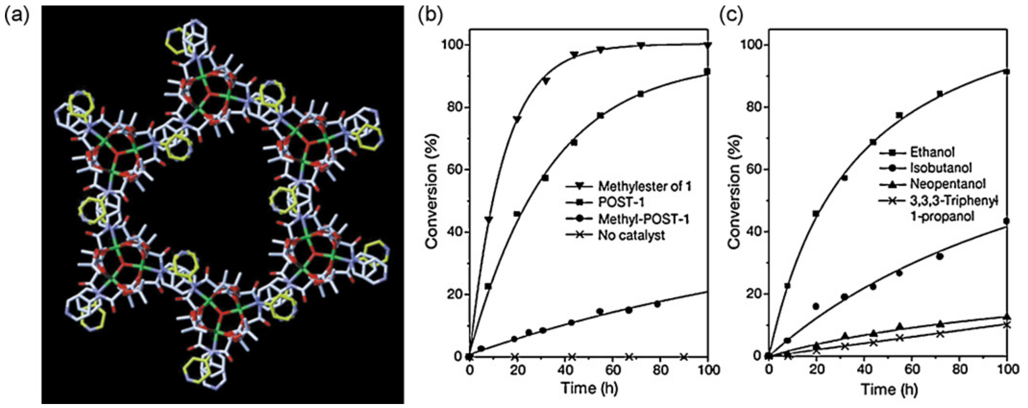

Fig. 21. (a) The hexagonal framework with large pores that is formed with the trinuclear secondary building units. (b) Catalytic activity of POST-1 in transesterification reactions with ethanol, and (c) with different alcohols. Reproduced with permission from Ref. [119].

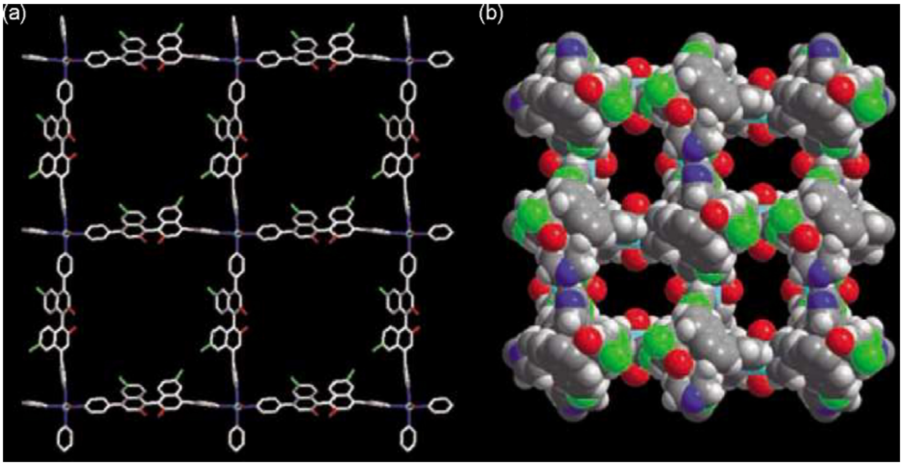

Fig. 22. (a) The 2D square grid in the crystal structure and (b) space-filling model as viewed down the *c* axis showing the chiral 1D channels of 13.5 Å × 13.5 Å in dimensions. Reproduced with permission from Ref. [120].

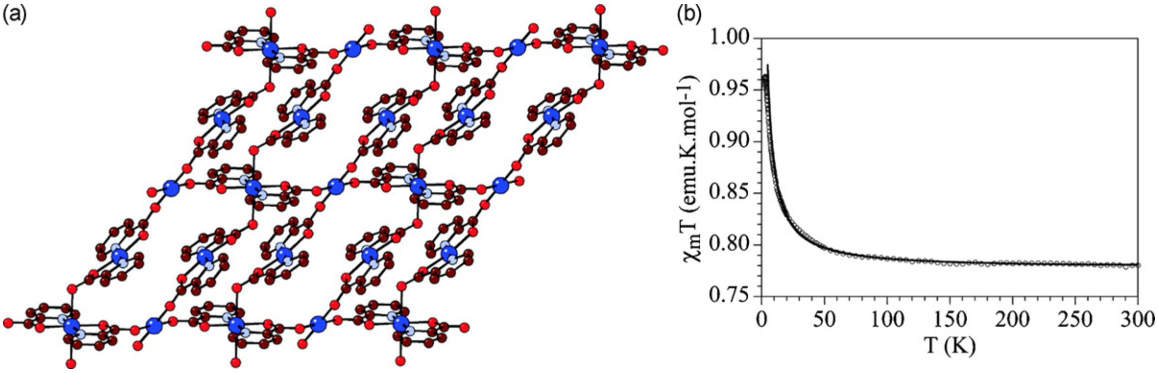

Fig. 23. (a) 2D layer [1 1 0] of the Cu^{II}-picolinate-bridged structure in $\{[Cu_2(pic)_3(H_2O)]ClO_4\}_n$. (b) Thermal variation of the product of the molar magnetic susceptibility and temperature ($\chi_m T$) for $\{[Cu_2(pic)_3(H_2O)]ClO_4\}_n$. Reproduced with permission from Ref. [129].

Another interesting example is TTTA·Cu(hfac)$_2$, an adduct of a metal complex and an organic free radical, reported by Fujita and Awaga [130]. In this structure TTTA ligands bridge Cu^{2+} ions to result in zigzag chains along the *b* axis, which are assembled together by two short contacts between the S atom on the dithiazolyl ring and the O atoms of Cu(hfac)$_2$ to form a 2D supramolecular layer (Fig. 24a). The magnetic measurements showed a ferromagnetic coupling ascribed to the coordination bond between Cu(hfac)$_2$ and TTTA and a weak antiferromagnetic coupling at low temperature due to the weak interaction between Cu(hfac)$_2$ and TTTA and/or the interchain interactions. Thus, the magnetic properties were interpreted in terms of a ferromagnetic dimer with a weak inter-dimer antiferromagnetic interaction.

6.2.2. Antiferromagnetic properties

Many MOFs have antiferromagnetic properties due to the antiparallel coupling of the spin metal ions or the organic free radical entities. Recently, Jia et al. [131] reported a 3D Mn^{2+} framework, Mn$_2$(tzc)$_2$(bpea), in which 2D layers with μ_3-tzc bridges are pillared by the bpea spacers to generate a 3D structure with a 3,4-

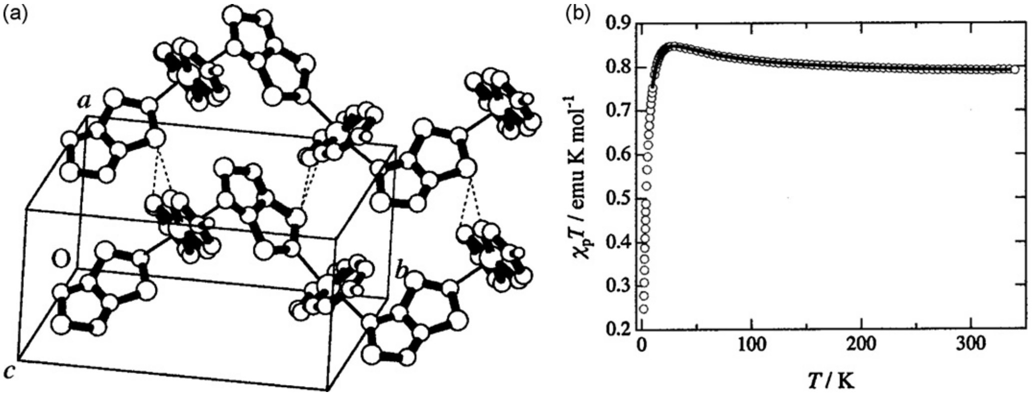

Fig. 24. (a) A view of the structure of TTTA·Cu(hfac)$_2$. The CF_3 groups of Cu(hfac)$_2$ are omitted for clarity. The interchain contacts are shown by the broken lines. (b) Temperature dependence of $\chi_p T$ for TTTA·Cu(hfac)$_2$. Reproduced with permission from Ref. [130].

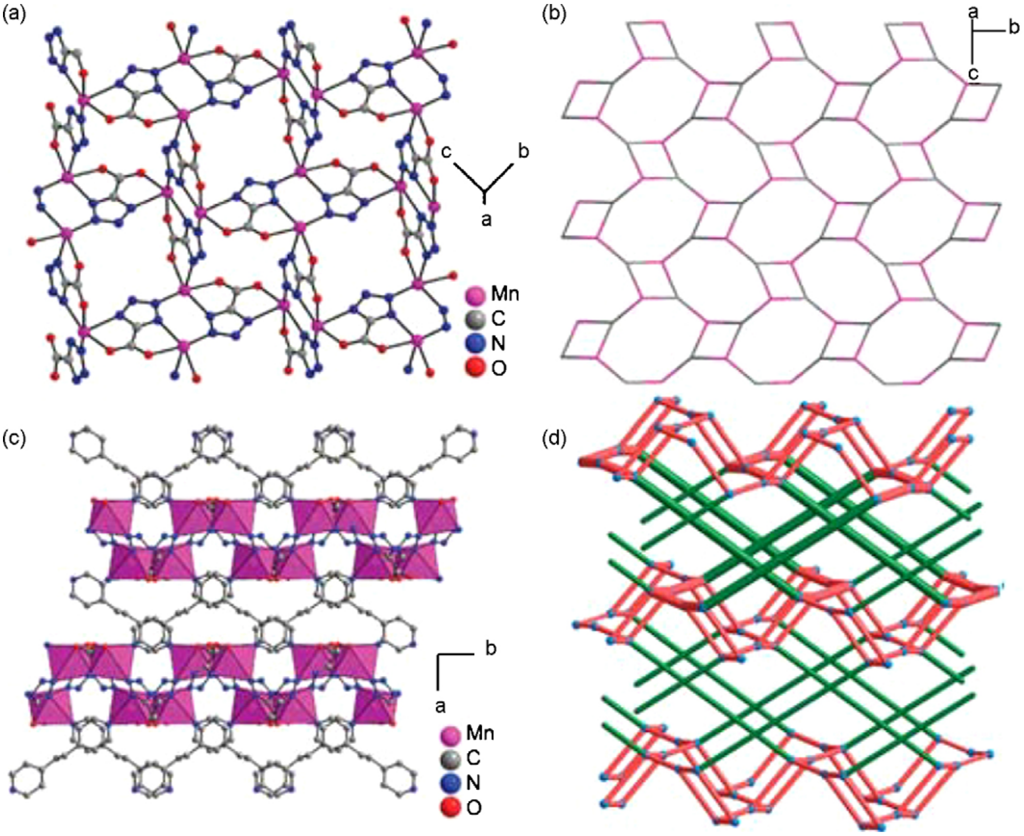

Fig. 25. The extended structure of $Mn_2(tzc)_2(bpea)$. (a) A 2D layer with tzc as μ_3-bridging ligands, (b) the 2D topology, (c) the 3D structure, and (d) the 3D topology with self-catenation highlighted by bold lines. Reproduced with permission from Ref. [131].

connected self-penetrating topology of $(4{\cdot}8^2 \times 10^3)(4{\cdot}8^2)$ (Fig. 25). The magnetic measurements revealed antiferromagnetic coupling between Mn^{2+} ions in this framework.

Yu et al. [132] also characterized the magnetic behavior of a non-interpenetrating chiral porous cobalt MOF, $Co_3(TATB)_2(H_2O)_2{\cdot}2DMA{\cdot}3H_2O$. The framework is composed of a trimetallic hourglass cluster linked by organic ligands with the cluster being responsible for the magnetic properties of the MOF. In the framework, every ligand pair is bound to three Co^{2+} clusters and every cluster connects with three ligand pairs to form a “propeller”. The clusters are extended by the TATB ligand pairs to form a non-interpenetrated (10, 3)-a framework containing chiral channels (Fig. 26a). Magnetic susceptibility measurements indicated that this MOF exhibited paramagnetic properties within measured temperature range 2–300 K, though antiferromagnetic coupling existed between neighboring Co^{2+} atoms (Fig. 26b).

6.2.3. *Ferrimagnetic properties*

In MOFs, the exchange coupling among paramagnetic centers typically leads to ferromagnetic or antiferromagnetic behavior, resulting in very few instances of ferromagnetic behavior. Usually, the ferrimagnetic systems contain two kinds of spin carriers

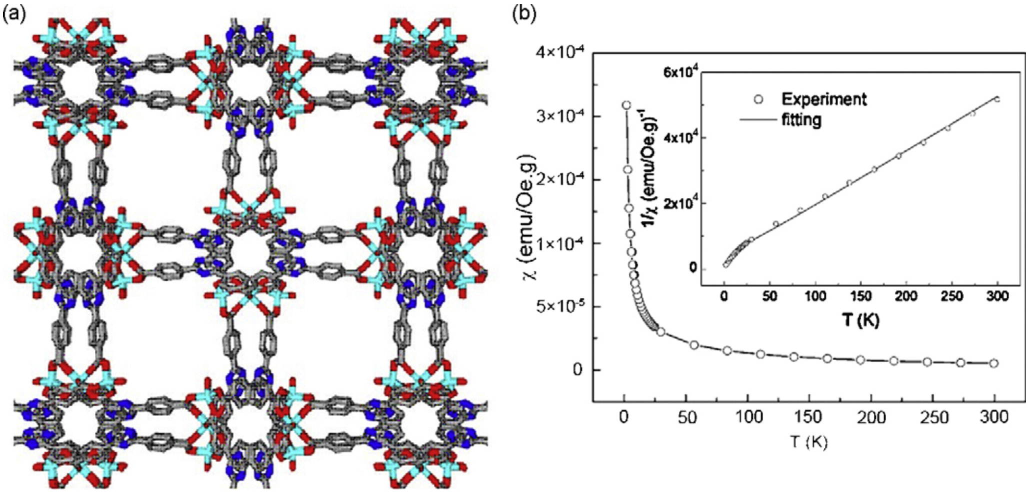

Fig. 26. (a) 3D framework structure of $Co_3(TATB)_2(H_2O)_2$. (b) Susceptibility as function of temperature (inset shows the $1/\chi$ *vs.* T curve along with a theoretical fitting). Reproduced with permission from Ref. [132].

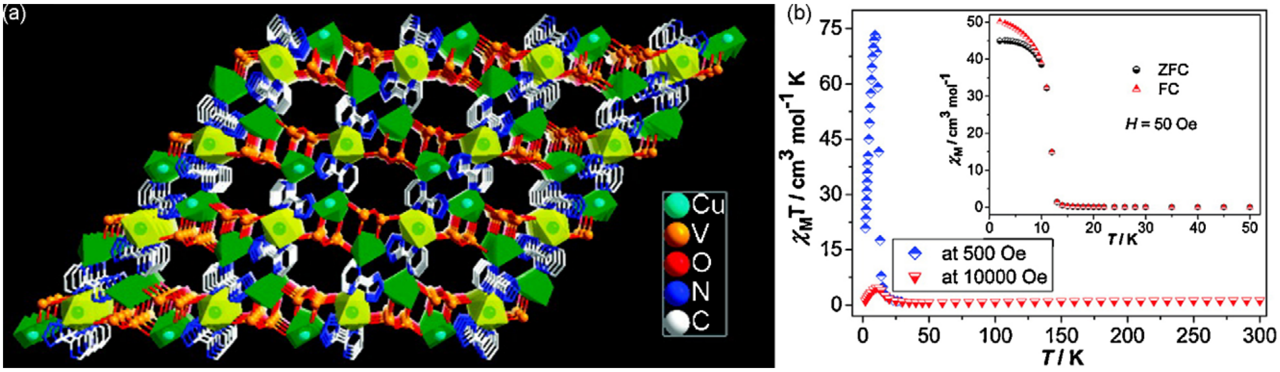

Fig. 27. (a) 3D framework structure of $Cu_3(\mathbf{L})_2(VO_3)_4$. (b) $\chi_m T$ *vs.* T plot at different fields and the zero field cooled (ZFC) and field cooled (FC) susceptibility plot for $Cu_3(\mathbf{L})_2(VO_3)_4$. Reproduced with permission from Ref. [133].

that alternate regularly and interact antiferromagnetically [121]. In contrast, homospin ferrimagnetic systems contain only one type of spin carrier that, in spite of the antiferromagnetic coupling, leads to a non-cancellation of spins as a result of a particular topological arrangement of the spins. Recently, Li et al. [133] reported a 3D homospin ferrimagnet, $Cu_3(\mathbf{L})_2(VO_3)_4$ ($\mathbf{L}$ = 5-(pyrimidin-2-yl)tetrazolate) constructed from $(VO_3{}^-)_n$ chains linking $([5\text{-(pyrimidin-2-yl)tetrazolate-}(Cu^{2+})_{1.5}]^{2+})_n$ layers (Fig. 27a). In the structure, there exist two crystallographically independent Cu^{2+} centers that are responsible for the unusual magnetic property. Magnetic measurements revealed this complex to be a ferrimagnet with T_N = 10 K (Fig. 27b). This framework can be seen as two lattices with an antiferromagnetic coupling between them that results in an uncompensated spin S = 1/2 per every three Cu^{2+} atoms. At low temperatures the uncompensated spins align parallel to each other, resulting in the ferromagnetic long-range order.

6.2.4. *Frustration and canting*

Frustrated magnetic materials have attracted much attention because the competing interactions in these materials can suppress or significantly reduce long-range magnetic ordering and may lead to unusual ground-state behaviors. The magnetic frustrations are usually observed in triangular or tetrahedral “plaquette” magnetic lattices [134–136]. Gao et al. [137] recently reported a Mn^{2+} complex, $Mn[Mn_3(\mu_3\text{-F})(bta)_3(H_2O)_6]_2$ which has a 2D frustrated lattice with alternating triangular motifs and mononuclear centers. Magnetic studies showed this compound to behave as a low-temperature antiferromagnet (Fig. 28). The stoichiometry and connecting mode of the mono- and tri-nuclear Mn^{2+} moieties in the 2D lattice led to an uncompensated spin moment, which caused the frustration.

In contrast to ferrimagnetism, residual spin resulting from perturbation of antiparallel or parallel coupling may induce spin canting. Asymmetric exchange interactions and single-ion magnetic anisotropy are the origins of this magnetic behavior [138]. Several MOFs have presented spin canted antiferromagnetic properties. Li et al. [139] reported a Co^{II} MOF, $Co_2(\mathbf{L})_2(H_2O)_2$ ($\mathbf{L}$ = 2,1,3-thiadiazole-4,5-dicarboxylate), which has a non-interpenetrated (10,3)-d (**utp**) topological network structure. It is interesting that in the crystallographic asymmetric unit there exist two unique

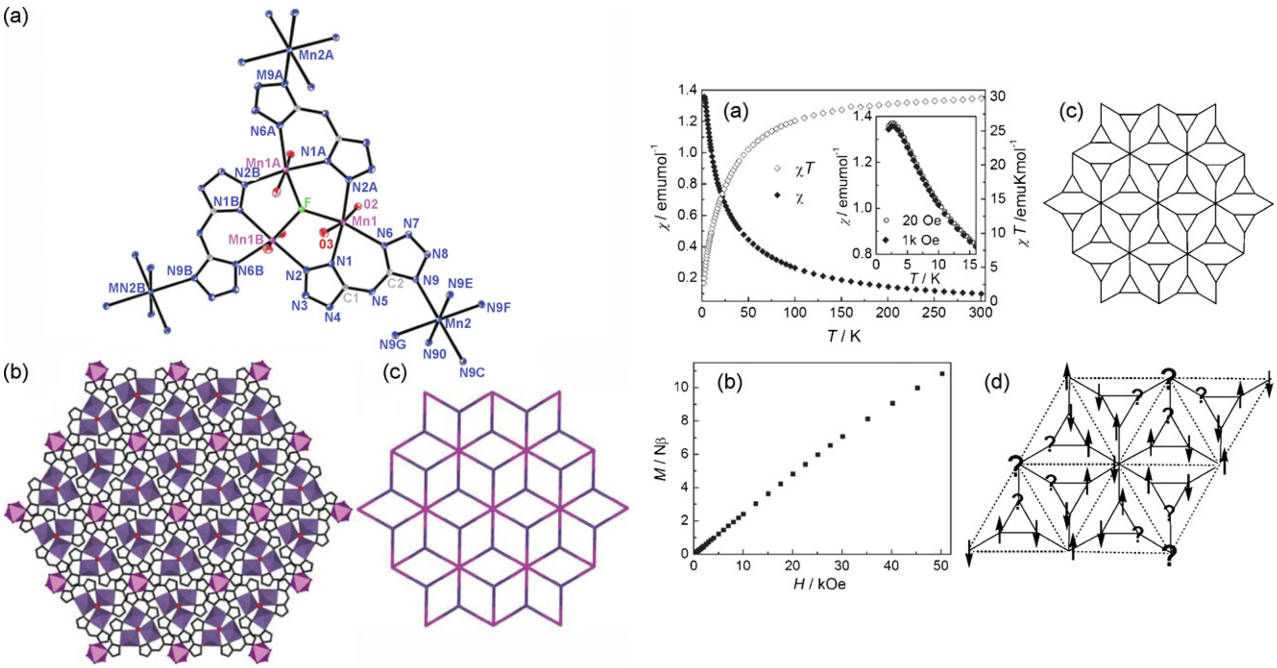

Fig. 28. Left: views of the structure of $Mn[Mn_3(\mu_3\text{-F})(bta)_3(H_2O)_6]_2$, showing (a) coordination environments of the metal ion and the ligand, (b) the 2D layer, and (c) the 3,6-connected net of the layer. Right: (a) temperature dependence of the susceptibility of $Mn[Mn_3(\mu_3\text{-F})(bta)_3(H_2O)_6]_2$. Inset: FC (20 and 1000 Oe) and ZFC (20 Oe) plots, (b) field-dependent magnetization, (c) schematic illustration of the 2D lattice, (d) a segment of the lattice illustrating the frustration and the triangular sublattice of Mn. Reproduced with permission from Ref. [137].

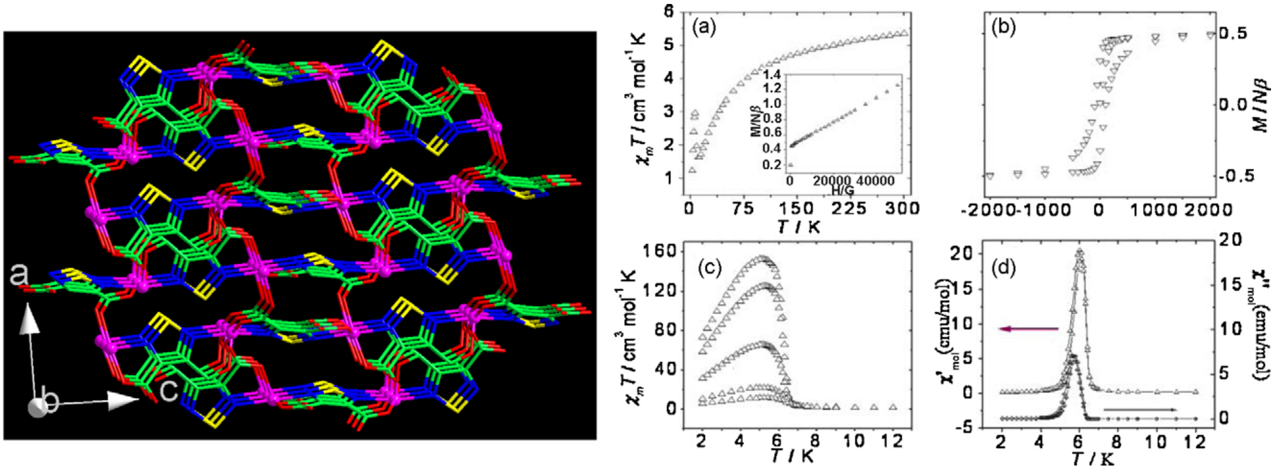

Fig. 29. Left: view of the 3D framework structure of $Co_2(\mathbf{L})_2(H_2O)_2$ (un-coordinated carboxylate O atoms and water molecules were omitted for clarity). Right: (a) $\chi_m T$ *vs.* T plot for $Co_2(\mathbf{L})_2(H_2O)_2$ (insert: plot of the reduced magnetization at 2 K), (b) hysteresis loop, (c) $\chi_m T$ *vs.* T plots at different fields (from 1000 to 50 G) in the low-temperature region, (d) plot of the ac susceptibility. Reproduced with permission from Ref. [139].

but chemically similar Co^{2+} ions, which were linked by ligands to form a 3D framework (Fig. 29, left). These two crystallographically different Co^{II} ions were determined to be responsible for the magnetic behaviors. Magnetic measurements showed that this complex takes on unexpected long-range magnetic ordering as shown in Fig. 29, right. Due to the shape of the $\chi_m T$ curve, ferromagnetic coupling between the Co^{2+} ions does not seem likely at high temperatures. There are different magnetic pathways – Co1–Co2, Co1–Co1, and Co2–Co2 – that have to be antiferromagnetic unless the *syn-anti* carboxylate coordinate mode is ferromagnetic yet very small in magnitude. Thus, the origin of this magnetic order can be attributed to a weak magnetic ordering, the so-called canting.

6.3. Spin-crossover and induced magnetic change in MOFs

Among efforts to introduce specific functions to MOFs, the incorporation of electronic switching centers is very important in the development of new advanced functional materials for molecular-scale switching devices. Spin-crossover centers represent a convenient, addressable molecular-scale magnetic switch in which d^4–d^7 transition metals can change between the high-spin and low-spin state in response to variation in temperature, pressure, or light irradiation [140]. Recently, Halder et al. [141] reported a nanoporous MOF, $Fe_2(azpy)_4(NCS)_4$·(guest) which has an interpenetrated "2D layer to 3D" framework structure containing electronic switching Fe^{2+} centers and displays reversible uptake

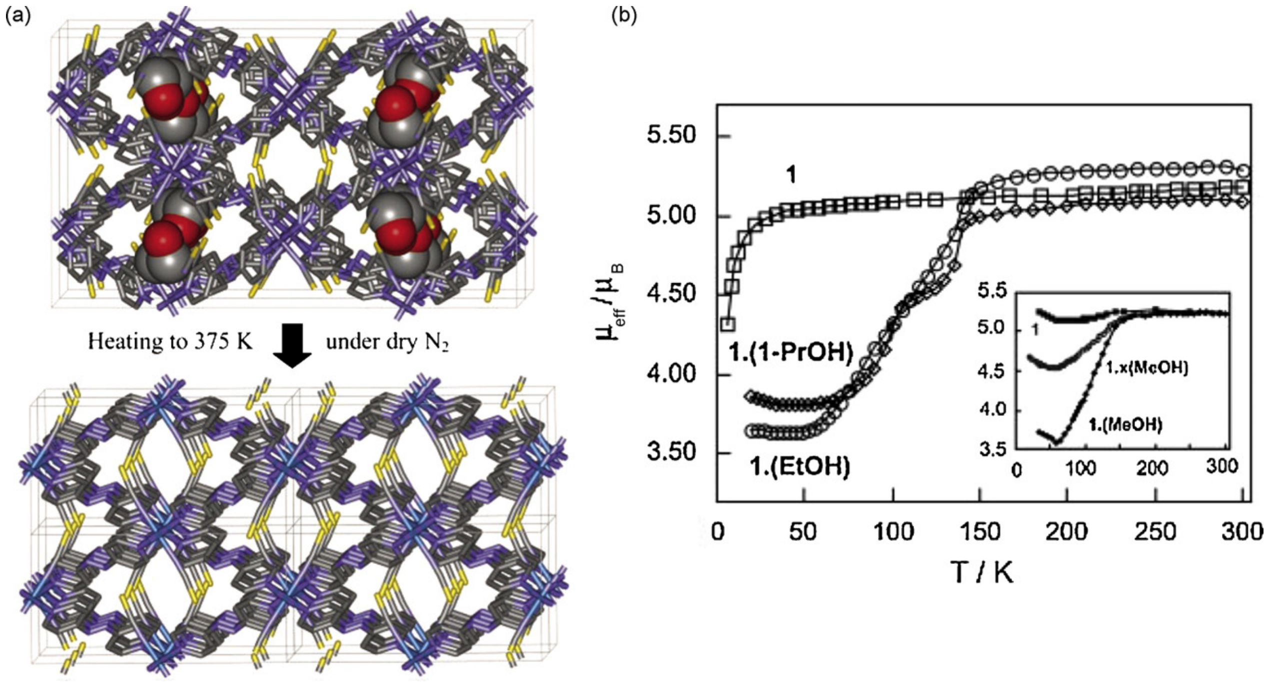

Fig. 30. (a) The structures of $Fe_2(azpy)_4(NCS)_4$·(EtOH) at 150 and 375 K. (b) The temperature-dependent magnetic moment of $Fe_2(azpy)_4(NCS)_4$·(guest), recorded on a single sample at different stages of guest desorption and resorption, showing 50% spin-crossover behavior between 50 and 150 K for the fully loaded phases and an absence of spin-crossover for the fully desorbed phase. The ethanol and methanol-loaded phases undergo a single step spin-crossover, whereas the 1-propanol adduct shows a two-step crossover with a plateau at 120 K. The inset shows the effect of partial and complete removal of methanol from $Fe_2(azpy)_4(NCS)_4$·(MeOH). Reproduced with permission from Ref. [141].

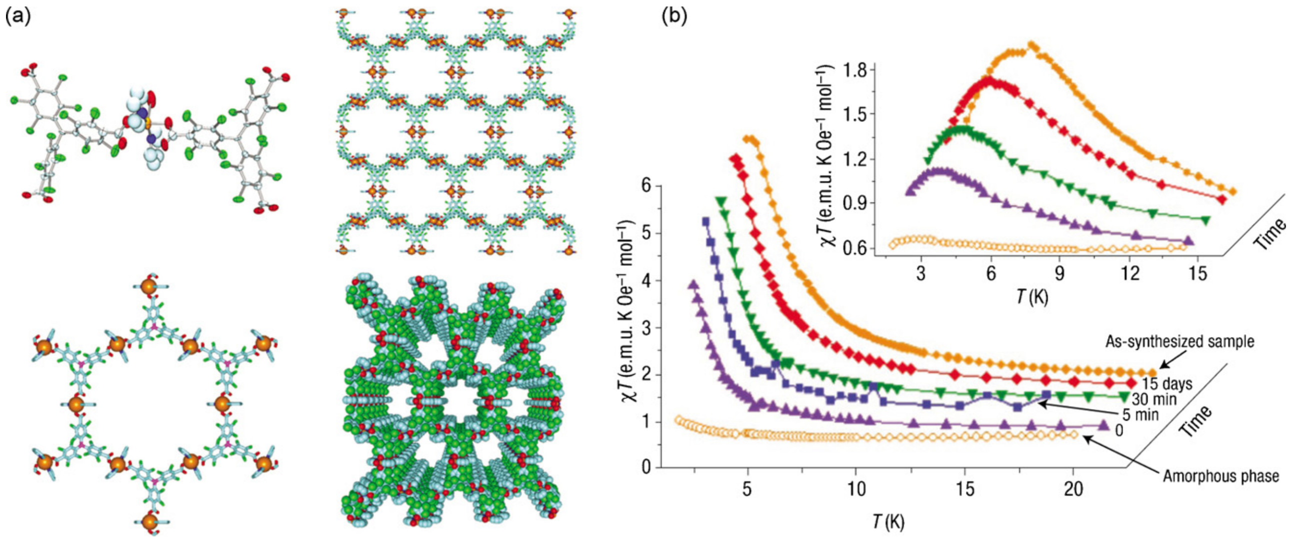

Fig. 31. (a) Structure of $Cu_3(PTMTC)_2(py)_6$. (b) Reversible magnetic behavior of the amorphous and evacuated phase in contact with ethanol liquid, as observed by plotting χT as a function of temperature T at a field of 1000 Oe. Inset: similar behavior at 10,000 Oe. Reproduced with permission from Ref. [143].

and release of guest molecules (Fig. 30a). The flexibility from the interpenetrated framework allows guest uptake and release, which in turn causes substantial changes in the local geometry at the Fe^{2+} centers. As a result, the presence of Fe^{2+} spin-crossover centers within the framework lattice led to the switching of this material: the sorbed phases undergoing "half-spin" crossovers, and the desorbed phase showing no switching property (Fig. 30b). This work has shown that MOF materials can incorporate an additional level of functionality, such as spin-transition associated with their porous natures to produce new, useful properties. Furthermore, the photomagnetic properties of a similar porous Fe^{2+} spin-crossover MOF, $Fe(NCS)_2(bped)_2{\cdot}3EtOH$ has been investigated by the same group [142].

Solvent-induced magnetic properties have also been observed in a nanoporous MOF structure, $Cu_3(PTMTC)_2(py)_6(EtOH)_2(H_2O)$, which was constructed by using a persistent organic free radical (PTMTC) functionalized with three carboxylic groups [143]. This MOF has a 2D layer structure extending along the *ab* plane composed of a honeycomb structure. These layers stack by using weak π–π and van der Waals interactions to form an open framework structure with hexagonal pores (Fig. 31a). It is even more interesting that this material shows a reversible and highly selective solvent-induced 'shrinking–breathing' process involving large volume changes (25–35%) that strongly influence its magnetic properties (Fig. 31b). Thus, this magnetic sponge-like behavior could be used as a new route towards magnetic solvent sensors.

7. Luminescence and sensors in MOFs

7.1. Introduction

The potential use of MOFs as luminescent materials has spurred much interest in the area [144,145]. These materials can be prepared by combining the luminescent metal ions or clusters and organic ligands, as well as special guest molecules [146].

7.2. Luminescence in MOFs

7.2.1. Luminescence in MOFs based on metal centers

Lanthanide metal ions have been widely used in MOF syntheses due to their coordination diversity and luminescent properties. Chandler et al. [147] reported a stepwise approach to synthesizing a MOF with photophysical properties through incorporation of lanthanide metal complexes in the framework, namely $[Ba_2(H_2O)_4[LnL_3(H_2O)_2](H_2O)_nCl]_\infty$ (L = 4,4′-disulfo-2,2′-bipyridine-N,N′-dioxide, Ln = Sm, Eu, Gd, Tb, Dy) (Fig. 32). A stepwise approach was used and allowed for an examination of the significance of the ratio of metal to organic building units in the preparation of a MOF containing lanthanide metal ions. By decreasing the ligand to metal ratio, a less dense, porous framework was prepared that maintained its luminescent characteristics. Additionally, metalloligands were referred to as building units for the development of lanthanide containing MOFs for use as sensing

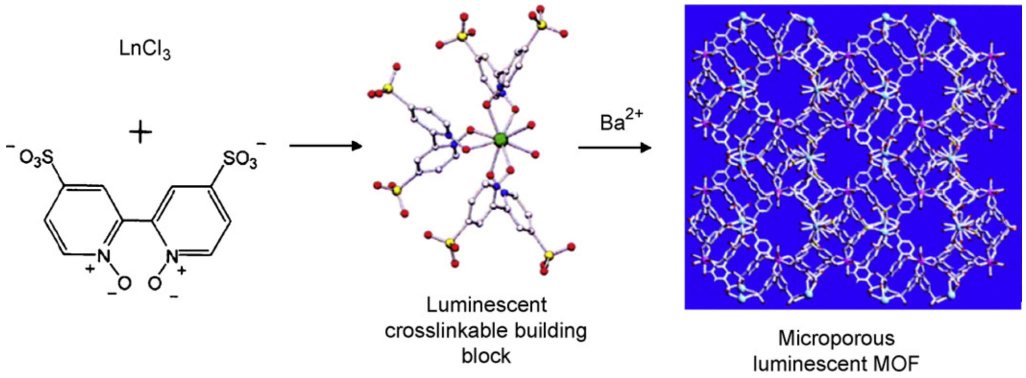

Fig. 32. Lanthanide metal complex and structure of $[Ba_2(H_2O)_4[LnL_3(H_2O)_2](H_2O)_nCl]_\infty$. Reproduced with permission from Ref. [147].

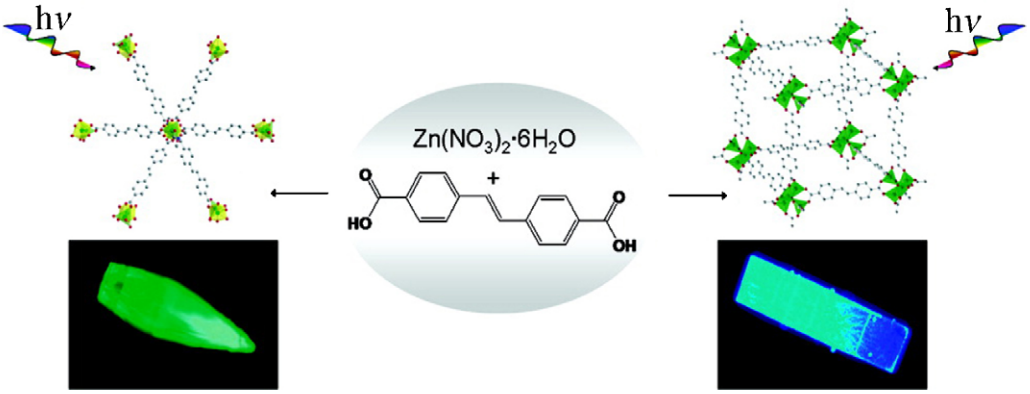

Fig. 33. Structure and luminescence properties of $Zn_3L_3(DMF)_2$ (left) and Zn_4OL_3 (right). Reproduced with permission from Ref. [150].

devices [148]. Proper selection of the linker is necessary to adequately shield the metal to prevent quenching of its luminescent properties.

de Lill et al. [149] reported in 2007 the synthesis and photoluminescent properties of a Eu MOF and a Eu/Tb mixed system MOF. In the mixed system, both Eu and Tb emissions were observed along with an increase in Eu emission intensity relative to the Eu MOF. This has been attributed to the Eu being sensitized by both the organic linkers and the Tb.

7.2.2. Luminescence in MOFs based on organic ligands

Two luminescent stilbene-based MOFs were prepared based on *trans*-4,4′-stilbene dicarboxylic acid (LH_2) and zinc nitrate in two different solvents. A 2D network structure $Zn_3L_3(DMF)_2$ was obtained in DMF, while a 3D porous framework structure Zn_4OL_3 resulted from DEF (Fig. 33) [150]. The optical properties of both demonstrate that the LH_2 organic ligand serves as the chromophore. In both cases, the rigidity of the stilbene ligand increases upon coordination to the metal center, resulting in increased emission lifetimes for the MOF crystals as compared to solutions of *trans*-stilbene.

Studies have also been conducted with luminescent organic linkers, such as H_2hfipbb as reported by Gándara et al. in 2007 [151]. As a ligand, hfipbb emits a blue-white color under UV light, which is slightly modified with the addition of different lanthanide metals, leading to the possible uses of these MOFs as diodes.

7.2.3. Luminescence based on guest molecules in MOFs

Huang et al. [152] reported a 3D porous MOF, $[Cd_3L_6](BF_4)_2(SiF_6)(OH)_2\cdot13.5H_2O$ (L = 2,6-di(4-triazolyl)pyridine), in which the guest species in the open channels can be removed and reintroduced reversibly without destroying the porous framework (Fig. 34a). Heating in air at different temperatures (180, 200, 225, 250 °C) for 1 day generated a series of dehydrated products. One of the dehydrated complexes was rehydrated when exposed to H_2O vapor for 1 or 2 days. The solid-state luminescence spectra of these complexes (Fig. 34b and c) revealed that guest molecules removed/rehydrated from the MOF undoubtedly influence the weak interactions between a ligand and a metal center. The work provides a convenient and effective route for tuning emissions between UV and visible wavelengths by controlling the number of guest molecules and may be useful for the design and fabrication of multifunctional luminescent materials.

7.3. Sensors in MOFs

The MOFs that possess luminescent properties together with size- or shape-selective sorption properties can be used as sensing devices [146].

7.3.1. Sensors for selective ion monitoring

Recently, Chen et al. [153] reported a prototype luminescent MOF, Tb(BTC)·G (MOF-76, G = guest solvent) (Fig. 35a). The luminescence properties of the anion incorporated Tb(BTC)·G (MOF-76b, G = methanol) microcrystalline solids were studied by immersing Tb(BTC) in methanolic solutions of different concentrations of NaX (X = F^-, Cl^-, and Br^-) and Na_2X (X = $CO_3{}^{2-}$ and $SO_4{}^{2-}$) (Fig. 35b). The results show that the luminescence intensity of the anion incorporated MOF-76b is significantly increased, particularly for the F^- incorporated MOF (Fig. 35c). The special properties underlying the potential of MOF-76 for the recognition and sensing of anions exhibit a high-sensitivity sensing function with respect to the fluoride anion.

Chen et al. [154] recently reported the synthesis of luminescent MOFs, $[Eu(pdc)_{1.5}(dmf)]\bullet(DMF)_{0.5}(H_2O)_{0.5}$ (**1**) (pdc = pyridine-3,5-

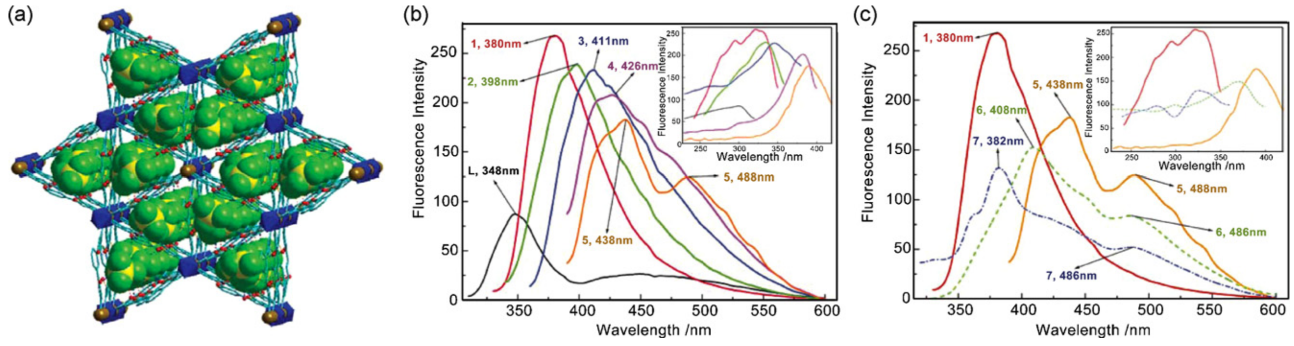

Fig. 34. (a) 3D framework of $[Cd_3L_6](BF_4)_2(SiF_6)(OH)_2\cdot13.5H_2O$ with the guest water molecules and anions in the cavities ($SiF_6{}^{2-}$, polyhedron, blue; $BF_4{}^-$, space filling, green and yellow); (b) Luminescence spectra of complexes with increasing dehydration, in the solid state at room temperature; (c) Luminescence spectra of complexes including those partially rehydrated, in the solid state at RT. Reproduced with permission from Ref. [152].

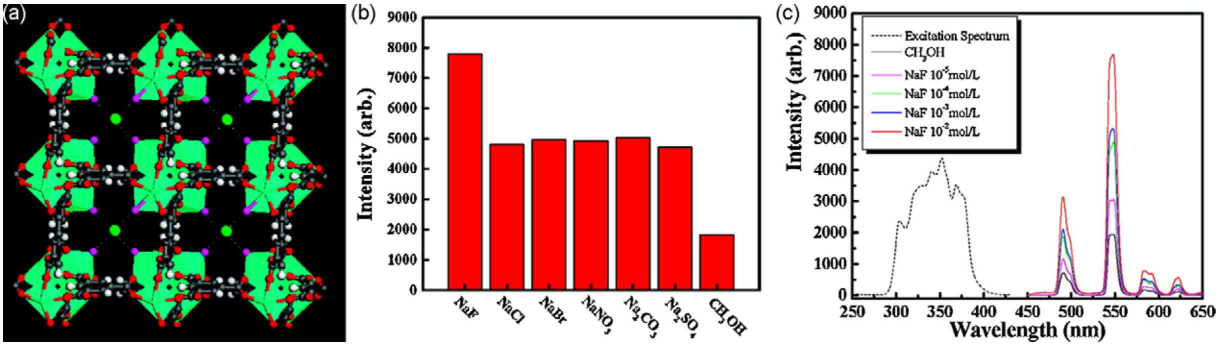

Fig. 35. (a) Crystal X-ray structure of MOF-76b containing NaF with the model of fluoride (green) at the center of the channel; (b) $^5D_4 \rightarrow {}^7F_5$ transition intensities of MOF-76b activated in different types of 10^{-2} M NaX and Na_2X methanol solution (excited and monitored at 353 and 548 nm, respectively); (c) Excitation (dotted) and PL spectra (solid) of MOF-76b solid activated in different concentrations of NaF methanol solution (excited and monitored at 353 and 548 nm, respectively). Reproduced with permission from Ref. [153].

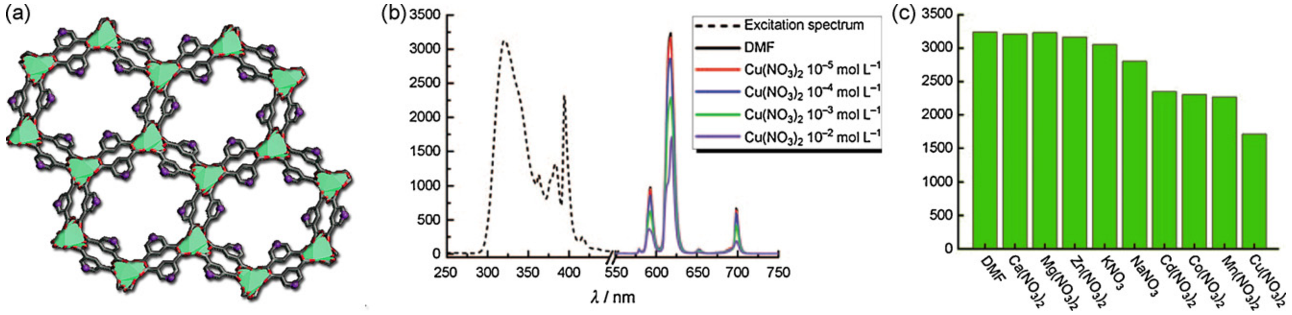

Fig. 36. (a) Crystal X-ray structure of **1** with immobilized Lewis basic pyridyl sites oriented towards pore centers; (b) The excitation (—) and PL spectra (- - -) of solid 1b activated in DMF solutions of $Cu(NO_3)_2$ at different concentrations (excited and monitored at 321 and 618 nm, respectively); (c) Comparison of the luminescence intensity of 1b incorporating different metal ions, activated in 10 mm DMF solutions of $M(NO_3)_x$. Adapted from Ref. [154].

dicarboxylate), with Lewis basic pyridyl sites for metal ion sensing (Fig. 36a). The luminescence characteristics of this MOF were studied as the pyridyl sites were coordinated to additional metal ions introduced in a DMF solution (Fig. 36b). It was found that the identity of the additional metal ion is very significant to the luminescence capability of the complex, with alkali and alkaline earth metals having little effect on the luminescence while other metal ions, such as Cu^{2+}, cause significant quenching (Fig. 36c).

7.3.2. *Sensors for the presence and/or types of guest/solvent molecules*

Chen et al. [155] reported a rare earth microporous MOF of Eu(BTC) (with open Eu^{3+} metal sites) (Fig. 38a). Within the MOF, ethanol, acetone, dimethyl formamide, and other small molecules exhibit different enhancing and quenching effects on the luminescence intensity (Fig. 37b and c). This MOF is suitable for the binding and sensing of small molecules by using the specific properties of luminescent open Eu^{3+} sites.

Using ultrasonic methods, Qiu et al. [156] obtained nanocrystals of a fluorescent microporous MOF, $Zn_3(BTC)_2{\cdot}12H_2O$ (Fig. 38a), and quantitatively analyzed the signals of organoamines in an acetonitrile solution using fluorescence spectrophotometric titrations. Remarkable changes of emission intensity (fluorescence quenching) were observed when the volume of ethylamine added into acetonitrile was changed (Fig. 38b). This fluorescence quenching suggests a high sensitivity to ethylamine and may lead to some highly sensitive sensors for organoamines.

7.3.3. *Sensors for stress-induced chemical detection*

Besides sensors for anions and guest molecules, MOFs can also be used for stress-induced chemical detection. Recent work by Allendorf et al. [157] demonstrated that the energy of molecular

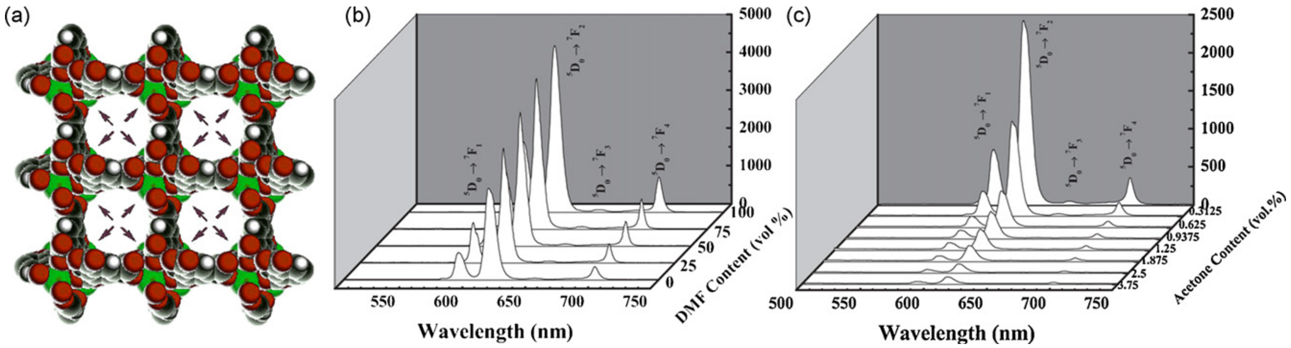

Fig. 37. (a) Structure of Eu(BTC) MOF viewed along the *c* axis, and accessible Eu^{3+} sites are shown by the pink arrows. The PL spectra in the presence of various content of (b) DMF and (c) acetone solvent, respectively (excited at 285 nm). Adapted from Ref. [155]. (For interpretation of the references to color in this figure legend, the reader is referred to the web version of the article.)

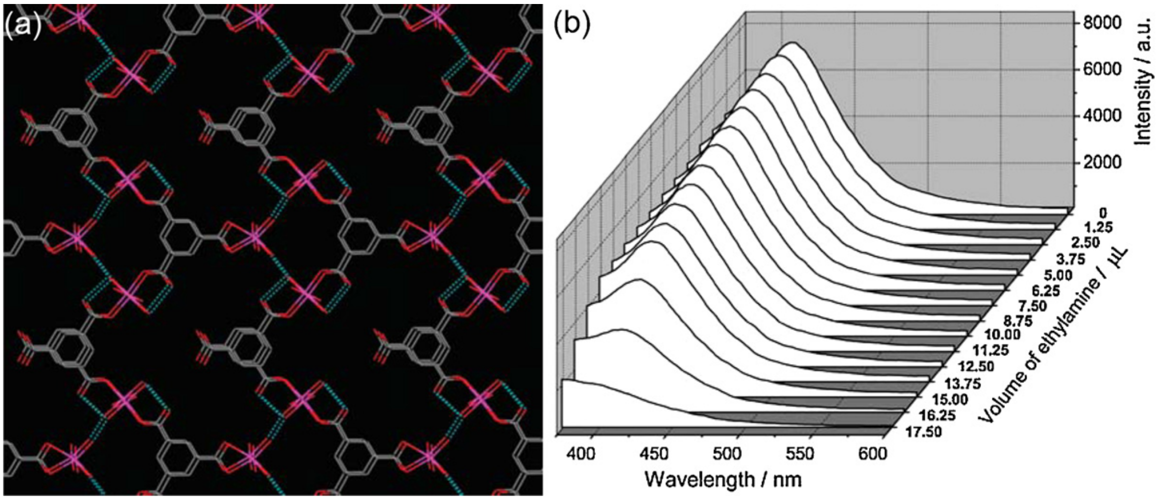

Fig. 38. (a) Molecular-packing diagram of $Zn_3(BTC)_2{\cdot}12H_2O$ viewed along the *c* axis; (b) Variation of emission spectra with the volume of ethylamine in 2 mL of acetonitrile (excited at 327 nm). Reproduced with permission from Ref. [156].

adsorption can be converted to mechanical energy to create a highly responsive, reversible, and selective sensor by integrating a thin film of MOF HKUST-1 with a microcantilever surface (Fig. 39a). This sensor responds to water (Fig. 39b), methanol, and ethanol vapors, but yields no response to either N_2 or O_2. This is the first report of the use of surface-enhanced Raman spectroscopy to characterize the structure of a MOF film.

7.3.4. Sensors for anisotropic photoluminescence probes

Harbuzaru et al. [158] presented new microporous Ln^{3+}-based materials, ITQMOF-1 and ITQMOF-2, based on the highly hydrophobic organic ligand Hfipbb. These MOFs show no quenching of photoluminescence in the presence of water (Fig. 40a and b), but a sharp decrease in photoluminescence in the presence of ethanol enables them to be used to sense ethanol in both air and water (Fig. 40c). It was also observed that the choice of Ln^{3+} metal is significant to the luminescent and magnetic properties of the MOFs. A ferromagnetic interaction between the Tb^{3+} ions and a green emission in UV light was observed for ITQMOF-1-Tb while ITQMOF-1-(5Eu–95Gd) showed an antiferromagnetic interaction between Gd^{3+} and a red emission in UV light (Fig. 40d).

8. Drug storage and delivery in MOFs

8.1. Introduction

The inability of conventional orally administered drugs to deliver medication at a controlled release rate has spawned much interest and research in novel methods for drug delivery. Developed delivery systems include polymeric-based systems, liposome-based systems, microporous zeolites, mesoporous silicon, and other mesoporous materials [159–162]. Essentially, these different delivery routes are classified into organic systems and inorganic systems. Organic systems benefit from a wide array of biocompatibility, the ability to uptake many drugs, yet lack a controlled release mechanism [163,164]. The inorganic delivery materials are able to deliver the adsorbed drugs at a controlled rate due to their ordered porous network, but have a decreased loading capacity [165,166].

8.2. Drug-delivery methods

Uhrich et al. provide a complete review of the organic polymeric drug-delivery materials [167]. Most inorganic delivery materials have a mesoporous structure to allow for optimal uptake and deliv-

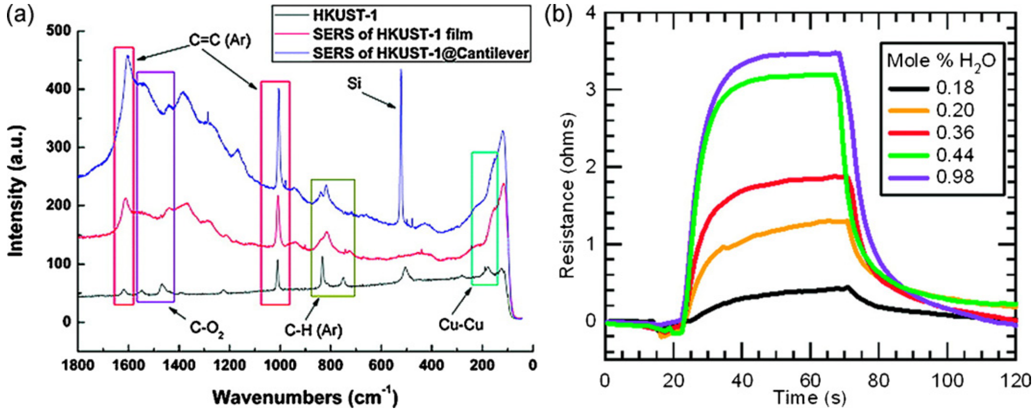

Fig. 39. (a) Verification of HKUST-1 on the microcantilever using SERS: (blue) SERS spectrum of HKUST-1 on a microcantilever; (red) SERS spectrum of an HKUST-1 film on a macroscopic substrate; (black) unenhanced Raman of a thick HKUST-1 layer used as a reference. Peaks labeled C–H(Ar) correspond to out-of-plane aromatic C–H bends; (b) Temporal response of the cantilever piezoresistive sensor to water vapor diluted in N_2 (room temperature, 1 atm). Reproduced with permission from Ref. [157]. (For interpretation of the references to color in this figure legend, the reader is referred to the web version of the article.)

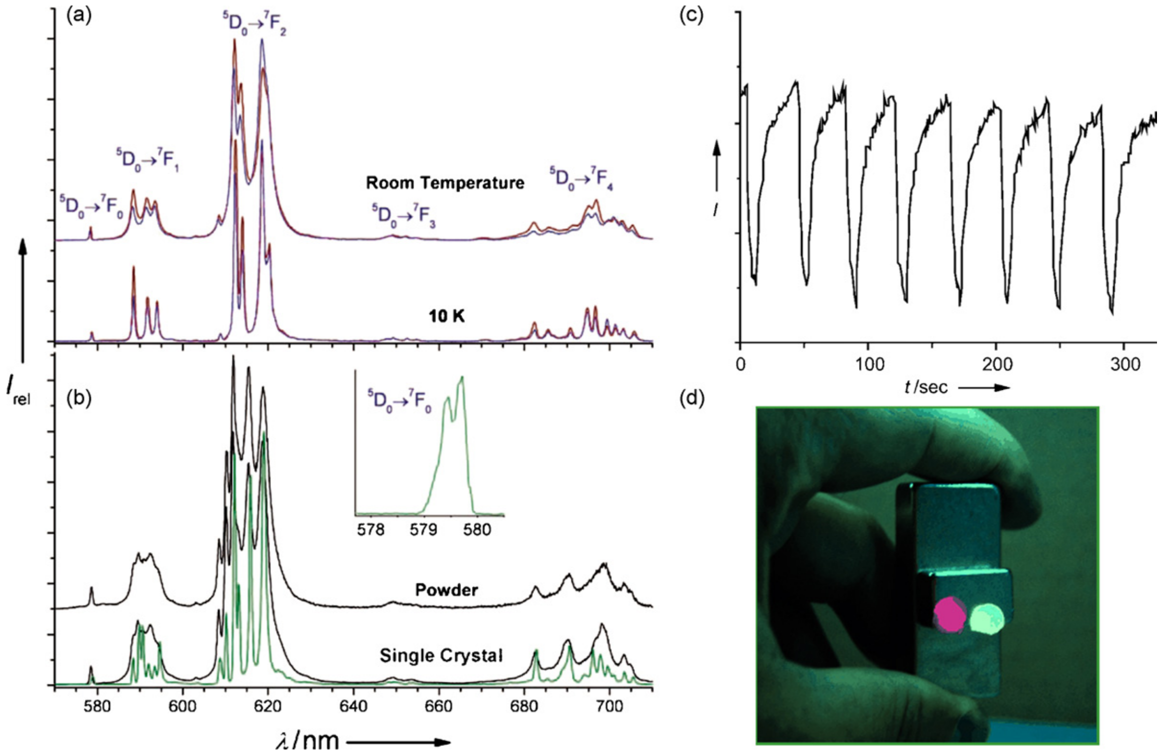

Fig. 40. (a) Emission spectra of a ITQMOF-1-(5Eu–95Gd) single crystal, recorded at room temperature and 10 K for two different orientations of the crystal relative to the detector (red line: vertical, blue line: horizontal, excited at 290 nm). (b) Emission spectra of ITQMOF-2-Eu powder and single crystal (oriented in the vertical position), recorded at room temperature (black line) and 10 K (green line). The inset shows an expansion of the $^5D_0 \to ^7F_0$ region at 10 K (excited at 290 nm). (c) Test for sensing capabilities of the ITQMOF-1-Eu material. Variation of the fluorescence signal intensity at 619 nm under alternating streams of air saturated with ethanol (signal intensity decreases) and ethanol-free air (signal intensity increases). (d) [Gd, Eu]- and [Tb]-containing materials under UV light and interacting with a magnet. Adapted from Ref. [158].

ery of drugs (microporous materials usually do not possess large enough apertures for useful drug delivery). Recently, Salonen et al. provided a review on the state of mesoporous silicon in drug delivery [160]. Zeolites in the mesoporous size range have also been studied for their application in drug delivery [161].

8.2.1. *Inorganic drug-delivery materials*

MCM-41 is an inorganic material composed of siloxane bridges with silanol groups available for interaction with guest species and for better control of the size of the pore. It has been one of the most intensely studied inorganic compounds for drug delivery because the pore walls allow for direct adsorption with no need for organic functionalization [166,168]. Munoz et al. provided the necessary background research for drug delivery in mesoporous silicate with their study of the release rate of ibuprofen in MCM-41 modified with aminopropyl groups [165]. Their findings established that the release rate of ibuprofen in MCM-41 without the addition of functional groups is independent of pore size so long as the mesoporous opening is larger than the delivered drug. Complete delivery of the drug occurs within two days. In addition, the functionalization of MCM-41 with organic silane groups can impact the amount of drug adsorbed, and therefore, the delivery rate [165].

8.2.2. *MOF drug-delivery materials*

As hybrid organic–inorganic compounds, MOFs present themselves as optimal drug-delivery materials due to the adjustability of the framework's functional groups and the tunable pore size. With MOFs, the benefits of using organic materials (biocompatibility and the ability to uptake large amounts of drugs) and inorganic materials (controlled release) may both be utilized. However, the main drawback of using MOFs is that the small pore size, with diameters that usually fall in the microporous range, limits the uptake and/or number of drug molecules that can be stored within the framework [169]. To solve this problem, MOFs containing pores in the mesoporous range must be synthesized.

Two such MOFs have been prepared by Horcajada et al. as MIL-100 and MIL-101 [169]. These structures proved suitable for drug delivery due to their well-defined, ordered porosity. MIL-100 contains pore diameters of 25–29 Å with pentagonal window openings of 4.8 Å and hexagonal windows of 8.6 Å while MIL-101 possesses pore sizes of 29–34 Å with a very large window opening of 12 Å for the pentagonal and 16 Å for the hexagonal windows [169]. MIL-100 was found to uptake 0.35 g ibuprofen/g dehydrated MIL-100 whereas MIL-101 was able to uptake 1.4 g ibuprofen/g dehydrated MIL-101. The difference can be explained by the size of ibuprofen (6 Å × 10.3 Å) which is able to fit in both the pentagonal and

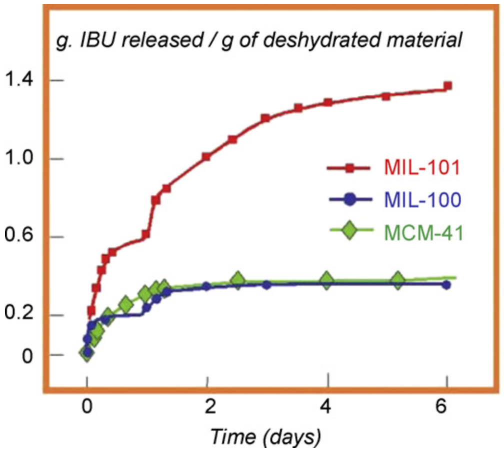

Fig. 41. The delivery rate of MIL-101, MIL-100, and MCM-41. Reproduced with permission from Ref. [3].

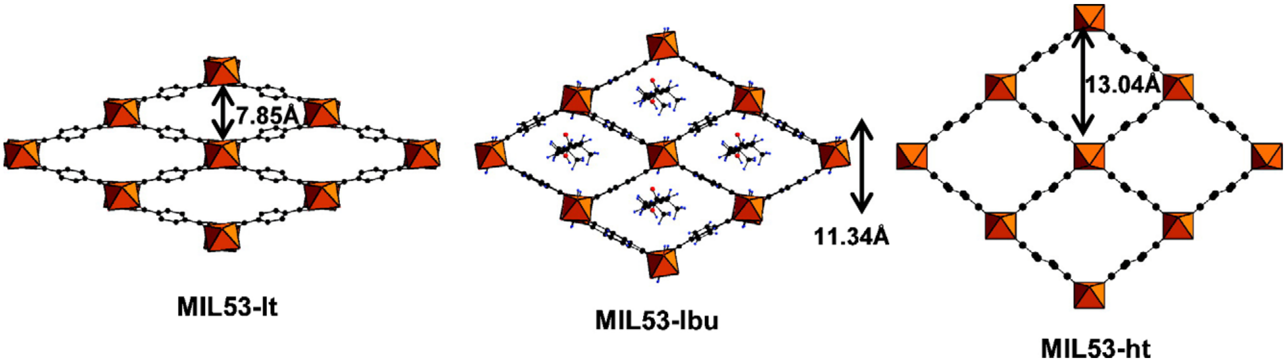

Fig. 42. The breathing effect of MIL-53(Cr) upon adsorption and release at high temperature. Reproduced with permission from Ref. [9].

hexagonal windows of MIL-101, but not into the smaller pentagonal window of MIL-100 [3,169]. Desorption rates for MIL-101 exceeded that of MIL-100 by six days *vs.* three days, respectively. The initial delivery mechanism consists of simple diffusion of weakly bonded molecules, whereas π–π interactions between the aromatic rings and the ibuprofen are responsible for the elongated delivery times [169]. Fig. 41 compares the release rate of MIL-101, MIL-100, and MCM-41, respectively.

In addition to MIL-100 and MIL-101, Loiseau et al. studied the drug-delivery rate of MIL-53, a flexible material known for its ability to expand its structure upon heating in what is termed a breathing effect (Fig. 42) [170]. MIL-53, with a maximum volume of approximately 1500 Å^3 at high temperature and full expansion, was able to uptake approximately 20 wt% of ibuprofen with a complete delivery taking approximately three weeks [9]. The long, steady delivery can be attributed to the flexibility of the framework to bend around the ibuprofen molecules to maximize the bonding interactions while still minimizing steric hindrance [9].

8.3. *Future work in drug delivery*

Although progress has been made, and MOFs have proven themselves suitable candidates for drug delivery, much research needs to be done to realize the full potential of MOFs as materials for drug delivery. With the increasing number of mesoporous MOFs being synthesized, drug delivery utilizing MOFs show promising potential.

9. Conclusion

From the foregoing discussions about potential application of MOFs, we can draw the following conclusions

(1) In the last decade, we have witnessed unprecedented rapid growth in the field of MOFs. Although early studies focused mainly on the structural diversity of MOFs, the research trend has now shifted towards various potential applications in the last five years.

(2) Gas storage of MOFs has become one of the focal points in MOF studies since 2003. Significant progress has been made in methane storage as the DOE goal at room temperature and applicable pressure has been surpassed for the first time. In hydrogen storage, although at 77 K and applicable pressure the uptake is high, the room temperature uptake is still very low. The key is to increase the hydrogen affinity of the frameworks so that at room temperature and applicable pressure, the U.S. DOE gravimetric and volumetric goals can be achieved.

(3) In selective gas adsorption, MOFs built from both flexible and rigid ligands have been found useful. Attention needs to be paid to the novel mesh-adjustable MOFs whose pore size can be tuned by changing temperature or pressure. Another trend is the application of MOFs in a number of important industrial applications such as methane purification and carbon dioxide sequestration.

(4) The use of MOFs for size-, shape-, and enantio-selective catalysis may become one of the most promising applications. MOF catalysis is different from both homogenous catalysis and surface heterogeneous catalysis. A reaction with known reactivity and selectivity may behave very differently in a confined space in a MOF.

(5) In the last several years, new applications of MOFs, such as those in the field of porous magnets, luminescent sensors, drug storage and delivery, and templated low-dimensional material preparation, have been demonstrated. Breakthroughs in the near future are possible with the continual development of these applications.

In conclusion, the MOF research community has made great progress in the last decade, yet we may have just seen the tip of the iceberg in respect to the application potential of MOFs. Many new types of applications will emerge as the research topic becomes more and more popular. The future of the field is indeed very bright.

Appendix A. Supplementary data

Supplementary data associated with this article can be found, in the online version, at doi:10.1016/j.ccr.2009.05.019.

References

[1] Z. Wang, G. Chen, K. Ding, Chem. Rev. 109 (2009) 322.
[2] J.-R. Li, R.J. Kuppler, H.C. Zhou, Chem. Soc. Rev. 38 (2009) 1477.
[3] G. Férey, Chem. Soc. Rev. 37 (2008) 191.
[4] B. McEnaney, E. Alain, Y.F. Yin, T.J. Mays, NATO Sci. Ser., Ser. E 374 (2001) 295.
[5] D.J. Borns, Theory Appl. Transp. Porous Media 20 (2006) 407.
[6] R.E. Morris, P.S. Wheatley, Angew. Chem. Int. Ed. Engl. 47 (2008) 4966.
[7] S.M. Manocha, Sadhana 28 (2003) 335.
[8] C. Serre, F. Millange, S. Surblé, G. Férey, Angew. Chem. Int. Ed. Engl. 43 (2004) 6285.
[9] P. Horcajada, C. Serre, G. Maurin, N.A. Ramsahye, F. Balas, M. Vallet-Regi, M. Sebban, F. Taulelle, G. Férey, J. Am. Chem. Soc. 130 (2008) 6774.
[10] Y.K. Park, S.B. Choi, H. Kim, K. Kim, B.H. Won, K. Choi, J.S. Choi, W.S. Ahn, N. Won, S. Kim, D.H. Jung, S.H. Choi, G.H. Kim, S.S. Cha, Y.H. Jhon, J.K. Yang, J. Kim, Angew. Chem. Int. Ed. Engl. 46 (2007) 8230.
[11] S. Kitagawa, R. Kitaura, S. Noro, Angew. Chem. Int. Ed. Engl. 43 (2004) 2334.
[12] G. Férey, J. Cejka, H. van Bekkum, A. Corma, F. Schüth, Stud. Surf. Sci. Catal., 168, 2007.
[13] D. Zhao, D.Q. Yuan, H.C. Zhou, Energy Environ. Sci. 1 (2008) 222.
[14] N.W. Ockwig, O. Delgado-Friedrichs, M. O'Keeffe, O.M. Yaghi, Acc. Chem. Res. 38 (2005) 176.
[15] R. Robson, Dalton Trans. (2008) 5113.
[16] M. O'Keeffe, M. Eddaoudi, H.L. Li, T. Reineke, O.M. Yaghi, J. Solid State Chem. 152 (2000) 3.
[17] P.M. Forster, P.M. Thomas, A.K. Cheetham, Chem. Mater. 14 (2002) 17.
[18] U. Mueller, M. Schubert, F. Teich, H. Puetter, K. Schierle-Arndt, J. Pastre, J. Mater. Chem. 16 (2006) 626.

[19] E. Biemmi, S. Christian, N. Stock, T. Bein, Micropor. Mesopor. Mater. 117 (2008) 111.
[20] G.A. Tompsett, W.C. Conner, K.S. Yngvesson, ChemPhysChem 7 (2006) 296.
[21] S.H. Jhung, J.W. Yoon, J.-S. Hwang, A.K. Cheetham, J.-S. Chang, Chem. Mater. 17 (2005) 4455.
[22] C.S. Collins, D. Sun, W. Liu, J.-L. Zuo, H.-C. Zhou, J. Mol. Struct. 890 (2008) 163.
[23] S.R. Batten, S.M. Neville, D.R. Turner, Coordination Polymers: Design, Analysis and Application, Royal Society of Chemistry, Cambridge, 2009, p. 471.
[24] D.J. Tranchemontagne, J.L. Mendoza-Cotres, M. O'Keeffe, O.M. Yaghi, Chem. Soc. Rev. 38 (2009) 1257.
[25] M. Eddaoudi, D.B. Moler, H. Li, B. Chen, T.M. Reineke, M. O'Keeffe, O.M. Yaghi, Acc. Chem. Res. 34 (2001) 319.
[26] O.M. Yaghi, M. O'Keeffe, N.W. Ockwig, H.K. Chae, M. Eddaoudi, J. Kim, Nature 423 (2003) 705.
[27] K.S.W. Sing, D.H. Everett, R.A.W. Haul, L. Moscou, R.A. Pierotti, J. Rouquerol, T. Siemieniewska, Pure Appl. Chem. 57 (1985) 603.
[28] S. Ma, H.-C. Zhou, J. Am. Chem. Soc. 128 (2006) 11734.
[29] S.Q. Ma, J. Eckert, P.M. Forster, J.W. Yoon, Y.K. Hwang, J.S. Chang, C.D. Collier, J.B. Parise, H.C. Zhou, J. Am. Chem. Soc. 130 (2008) 15896.
[30] Z. Wang, S.M. Cohen, Chem. Soc. Rev. 38 (2009) 1315.
[31] A.W.C. van den Berg, C.O. Areán, Chem. Commun. (2008) 668.
[32] DOE Office of Energy Efficiency and Renewable Energy Hydrogen, Fuel Cells & Infrastructure Technologies Program Multi-Year Research, Development and Demonstration Plan, available at: http://www.eere.energy.gov/hydrogenandfuelcells/mypp.
[33] L. Schlapbach, A. Züttel, Nature 414 (2001) 353.
[34] S.I. Orimo, Y. Nakamori, J.R. Eliseo, A. Züttel, C.M. Jensen, Chem. Rev. 107 (2007) 4111.
[35] N.L. Rosi, J. Eckert, M. Eddaoudi, D.T. Vodak, J. Kim, M. O'Keeffe, O.M. Yaghi, Science 300 (2003) 1127.
[36] J.L.C. Rowsell, O.M. Yaghi, Angew. Chem. Int. Ed. Engl. 44 (2005) 4670.
[37] V.I. Isaeva, L.M. Kustov, Russ. J. Gen. Chem. 77 (2007) 721.
[38] M. Hirscher, B. Panella, Scr. Mater. 56 (2007) 809.
[39] X. Lin, J.H. Jia, P. Hubberstey, M. Schröder, N.R. Champness, CrystEngComm 9 (2007) 438.
[40] D.J. Collins, H.C. Zhou, J. Mater. Chem. 17 (2007) 3154.
[41] M. Dincă, J.R. Long, Angew. Chem. Int. Ed. Engl. 47 (2008) 6766.
[42] A.G. Wong-Foy, A.J. Matzger, O.M. Yaghi, J. Am. Chem. Soc. 128 (2006) 3494.
[43] H. Furukawa, M.A. Miller, O.M. Yaghi, J. Mater. Chem. 17 (2007) 3197.
[44] S.K. Bhatia, A.L. Myers, Langmuir 22 (2006) 1688.
[45] Q. Wang, J.K. Johnson, J. Chem. Phys. 110 (1999) 577.
[46] J.H. Luo, H.W. Xu, Y. Liu, Y.S. Zhao, L.L. Daemen, C. Brown, T.V. Timofeeva, S.Q. Ma, H.C. Zhou, J. Am. Chem. Soc. 130 (2008) 9626.
[47] B. Kesanli, Y. Cui, M.R. Smith, E.W. Bittner, B.C. Bockrath, W.B. Lin, Angew. Chem. Int. Ed. Engl. 44 (2005) 72.
[48] D.H. Jung, D. Kim, T.B. Lee, S.B. Choi, J.H. Yoon, J. Kim, K. Choi, S.H. Choi, J. Phys. Chem. B 110 (2006) 22987.
[49] S.Q. Ma, D.F. Sun, M. Ambrogio, J.A. Fillinger, S. Parkin, H.C. Zhou, J. Am. Chem. Soc. 129 (2007) 1858.
[50] M. Dincă, A. Dailly, C. Tsay, J.R. Long, Inorg. Chem. 47 (2008) 11.
[51] P. Ryan, L.J. Broadbelt, R.Q. Snurr, Chem. Commun. (2008) 4132.
[52] B. Chen, X. Zhao, A. Putkham, K. Hong, E.B. Lobkovsky, E.J. Hurtado, A.J. Fletcher, K.M. Thomas, J. Am. Chem. Soc. 130 (2008) 6411.
[53] J.G. Vitillo, L. Regli, S. Chavan, G. Ricchiardi, G. Spoto, P.D.C. Dietzel, S. Bordiga, A. Zecchina, J. Am. Chem. Soc. 130 (2008) 8386.
[54] Y.G. Lee, H.R. Moon, Y.E. Cheon, M.P. Suh, Angew. Chem. Int. Ed. Engl. 47 (2008) 7741.
[55] H. Chun, J. Am. Chem. Soc. 130 (2008) 800.
[56] X.S. Wang, S.Q. Ma, P.M. Forster, D.Q. Yuan, J. Eckert, J.J. López, B.J. Murphy, J.B. Parise, H.C. Zhou, Angew. Chem. Int. Ed. Engl. 47 (2008) 7263.
[57] Y.Y. Sun, Y.H. Kim, S.B. Zhang, J. Am. Chem. Soc. 129 (2007) 12606.
[58] W. Zhou, H. Wu, T. Yildirim, J. Am. Chem. Soc. 130 (2008) 15268.
[59] H. Irving, R.J.P. Williams, J. Chem. Soc. (1953) 3192.
[60] W. Zhou, T. Yildirim, J. Phys. Chem. C 112 (2008) 8132.
[61] A. Blomqvist, C.M. Araújo, P. Srepusharawoot, R. Ahuja, Proc. Natl. Acad. Sci. U.S.A. 104 (2007) 20173.
[62] S.S. Han, W.A. Goddard, J. Am. Chem. Soc. 129 (2007) 8422.
[63] E. Klontzas, A. Mavrandonakis, E. Tylianakis, G.E. Froudakis, Nano Lett. 8 (2008) 1572.
[64] P. Dalach, H. Frost, R.Q. Snurr, D.E. Ellis, J. Phys. Chem. C 112 (2008) 9278.
[65] S.S. Kaye, J.R. Long, J. Am. Chem. Soc. 130 (2008) 806.
[66] K.L. Mulfort, J.T. Hupp, J. Am. Chem. Soc. 129 (2007) 9604.
[67] K.L. Mulfort, J.T. Hupp, Inorg. Chem. 47 (2008) 7936.
[68] K.L. Mulfort, T.M. Wilson, M.R. Wasielewski, J.T. Hupp, Langmuir 25 (2009) 503.
[69] S. Yang, X. Lin, A.J. Blake, K.M. Thomas, P. Hubberstey, N.R. Champness, M. Schröder, Chem. Commun. (2008) 6108.
[70] L.F. Wang, R.T. Yang, Energy Environ. Sci. 1 (2008) 268.
[71] Y.W. Li, R.T. Yang, J. Am. Chem. Soc. 128 (2006) 8136.
[72] S. Proch, J. Herrmannsdörfer, R. Kempe, C. Kern, A. Jess, L. Seyfarth, J. Senker, Chem.-Eur. J. 14 (2008) 8204.
[73] Y.L. Liu, J.F. Eubank, A.J. Cairns, J. Eckert, V.C. Kravtsov, R. Luebke, M. Eddaoudi, Angew. Chem. Int. Ed. Engl. 46 (2007) 3278.
[74] D.F. Sava, V.C. Kravtsov, F. Nouar, L. Wojtas, J.F. Eubank, M. Eddaoudi, J. Am. Chem. Soc. 130 (2008) 3768.
[75] J.L. Belof, A.C. Stern, M. Eddaoudi, B. Space, J. Am. Chem. Soc. 129 (2007) 15202.
[76] A. Kuc, T. Heine, G. Seifert, H.A. Duarte, Chem.-Eur. J. 14 (2008) 6597.
[77] A.P. Nelson, O.K. Farha, K.L. Mulfort, J.T. Hupp, J. Am. Chem. Soc. 131 (2009) 458.
[78] E. Poirier, A. Dailly, J. Phys. Chem. C 112 (2008) 13047.
[79] V.C. Menon, S. Komarneni, J. Porous Mater. 5 (1998) 43.
[80] T. Düren, L. Sarkisov, O.M. Yaghi, R.Q. Snurr, Langmuir 20 (2004) 2683.
[81] M. Kondo, T. Yoshitomi, K. Seki, H. Matsuzaka, S. Kitagawa, Angew. Chem. Int. Ed. Engl. 36 (1997) 1725.
[82] S.Q. Ma, D.F. Sun, J.M. Simmons, C.D. Collier, D.Q. Yuan, H.C. Zhou, J. Am. Chem. Soc. 130 (2008) 1012.
[83] I. Senkovska, S. Kaskel, Micropor. Mesopor. Mater. 112 (2008) 108.
[84] M. Kondo, T. Okubo, A. Asami, S. Noro, T. Yoshitomi, S. Kitagawa, T. Ishii, H. Matsuzaka, K. Seki, Angew. Chem. Int. Ed. Engl. 38 (1999) 140.
[85] S. Noro, S. Kitagawa, M. Kondo, K. Seki, Angew. Chem. Int. Ed. Engl. 39 (2000) 2082.
[86] M. Eddaoudi, J. Kim, N. Rosi, D. Vodak, J. Wachter, M. O'Keeffe, O.M. Yaghi, Science 295 (2002) 469.
[87] S. Bourrelly, P.L. Llewellyn, C. Serre, F. Millange, T. Loiseau, G. Férey, J. Am. Chem. Soc. 127 (2005) 13519.
[88] X.S. Wang, S.Q. Ma, K. Rauch, J.M. Simmons, D.Q. Yuan, X.P. Wang, T. Yildirim, W.C. Cole, J.J. López, A. de Meijere, H.C. Zhou, Chem. Mater. 20 (2008) 3145.
[89] C.J. King, Separation Progress, 2nd ed., McGraw Hill, New York, 1980.
[90] R.T. Yang, Adsorbents: Fundamentals and Applications, John Wiley & Sons, Hoboken, 2003.
[91] B.L. Karger, R.L. Snyder, H. Horvath, An Introduction to Separation Science, Wiley, New York, 1973.
[92] R. Xu, W. Pang, J. Yu, Q. Huo, J. Chen, Chemistry of Zeolites and Related Porous Materials: Synthesis and Structure, John Wiley & Sons (Asia) Pet Ltd., Singapore, 2007.
[93] R.T. Yang, Gas Separation by Adsorption Progress, Butterworth, Boston, 1987.
[94] F. Rouquerol, I. Rouquerol, K. Sing, Adsorption by Powders and Porous Solids Principles, Methodology and Applications, Academic Press, London, 1999.
[95] S. Ma, D. Sun, X.-S. Wang, H.-C. Zhou, Angew. Chem. Int. Ed. Engl. 46 (2007) 2458.
[96] S.Q. Ma, X.S. Wang, C.D. Collier, E.S. Manis, H.C. Zhou, Inorg. Chem. 46 (2007) 8499.
[97] M. Dincă, J.R. Long, J. Am. Chem. Soc. 127 (2005) 9376.
[98] S.Q. Ma, X.S. Wang, D.Q. Yuan, H.C. Zhou, Angew. Chem. Int. Ed. Engl. 47 (2008) 4130.
[99] Y.E. Cheon, M.P. Suh, Chem.-Eur. J. 14 (2008) 3961.
[100] M. Dincă, A.F. Yu, J.R. Long, J. Am. Chem. Soc. 128 (2006) 8904.
[101] R. Kitaura, K. Seki, G. Akiyama, S. Kitagawa, Angew. Chem. Int. Ed. Engl. 42 (2003) 444.
[102] K. Seki, Phys. Chem. Chem. Phys. 4 (2002) 1968.
[103] D. Tanaka, K. Nakagawa, M. Higuchi, S. Horike, Y. Kubota, L.C. Kobayashi, M. Takata, S. Kitagawa, Angew. Chem. Int. Ed. Engl. 47 (2008) 3914.
[104] B. Chen, C. Liang, J. Yang, D.S. Contreras, Y.L. Clancy, E.B. Lobkovsky, O.M. Yaghi, S. Dai, Angew. Chem. Int. Ed. Engl. 45 (2006) 1390.
[105] N.Y. Chen, W.E. Garwood, F.G. Dwyer, Shape-Selective Catalysis in Industrial Applications, Marcel Dekker, New York, 1989.
[106] H. Guo, G. Zhu, I.J. Hewitt, S. Qiu, J. Am. Chem. Soc. 131 (2009) 1646.
[107] S. Couck, J.F.M. Denayer, G.V. Baron, T. Rémy, J. Gascon, F. Kapteijn, J. Am. Chem. Soc. 131 (2009) 6326.
[108] H. Kim, D.G. Samsonenko, M. Yoon, J.W. Yoon, Y.K. Hwang, J.-S. Chang, K. Kim, Chem. Commun. (2008) 4697.
[109] J.-P. Zhang, X.-M. Chen, J. Am. Chem. Soc. 130 (2008) 6010.
[110] S. Ma, D. Sun, D. Yuan, X.-S. Wang, H.-C. Zhou, J. Am. Chem. Soc. 131 (2009) 6445.
[111] R.Q. Zou, H. Sakurai, Q. Xu, Angew. Chem. Int. Ed. Engl. 45 (2006) 2542.
[112] F. Gándara, B. Gornez-Lor, E. Gutiérrez-Puebla, M. Iglesias, M.A. Monge, D.M. Proserpio, N. Snejko, Chem. Mater. 20 (2008) 72.
[113] M.H. Alkordi, Y.L. Liu, R.W. Larsen, J.F. Eubank, M. Eddaoudi, J. Am. Chem. Soc. 130 (2008) 12639.
[114] F. Schröder, D. Esken, M. Cokoja, M.W.E. van den Berg, O.I. Lebedev, G. van Tendeloo, B. Walaszek, G. Buntkowsky, H.H. Limbach, B. Chaudret, R.A. Fischer, J. Am. Chem. Soc. 130 (2008) 6119.
[115] Y.K. Hwang, D.Y. Hong, J.S. Chang, S.H. Jhung, Y.K. Seo, J. Kim, A. Vimont, M. Daturi, C. Serre, G. Férey, Angew. Chem. Int. Ed. Engl. 47 (2008) 4144.
[116] M.J. Ingleson, J.P. Barrio, J. Bacsa, C. Dickinson, H. Park, M.J. Rosseinsky, Chem. Commun. (2008) 1287.
[117] S. Hasegawa, S. Horike, R. Matsuda, S. Furukawa, K. Mochizuki, Y. Kinoshita, S. Kitagawa, J. Am. Chem. Soc. 129 (2007) 2607.
[118] S. Horike, M. Dincă, K. Tamaki, J.R. Long, J. Am. Chem. Soc. 130 (2008) 5854.
[119] J.S. Seo, D. Whang, H. Lee, S.I. Jun, J. Oh, Y.J. Jeon, K. Kim, Nature 404 (2000) 982.
[120] C.D. Wu, W.B. Lin, Angew. Chem. Int. Ed. Engl. 46 (2007) 1075.
[121] C. Mathoniere, J.P. Sutter, J.V. Yakhmi, Magnetism: Molecules to Materials II, Wiley-VCH, Weinheim, 2003, p. 1.
[122] M. Kurmoo, Chem. Soc. Rev. 38 (2009) 1353.
[123] J. Ribas, A. Escuer, M. Monfort, R. Vicente, R. Cortes, L. Lezama, T. Rojo, Coord. Chem. Rev. 195 (1999) 1027.
[124] X.Y. Wang, Z.M. Wang, S. Gao, Chem. Commun. (2008) 281.
[125] L.M.C. Beltran, J.R. Long, Acc. Chem. Res. 38 (2005) 325.
[126] J.S. Miller, Dalton Trans. (2006) 2742.
[127] E. Pardo, R. Ruiz-Garcia, J. Cano, X. Ottenwaelder, R. Lescouezec, Y. Journaux, F. Lloret, M. Julve, Dalton Trans. (2008) 2780.

[128] D. Maspoch, D. Ruiz-Molina, J. Veciana, J. Mater. Chem. 14 (2004) 2713.
[129] C. Biswas, P. Mukherjee, M.G.B. Drew, C.J. Gomez-Garcia, J.M. Clemente-Juan, A. Ghosh, Inorg. Chem. 46 (2007) 10771.
[130] W. Fujita, K. Awaga, J. Am. Chem. Soc. 123 (2001) 3601.
[131] Q.X. Jia, Y.Q. Wang, Q. Yue, Q.L. Wang, E.Q. Gao, Chem. Commun. (2008) 4894.
[132] C.T. Yu, S.Q. Ma, M.J. Pechan, H.C. Zhou, J. Appl. Phys. 101 (2007) 09E108.
[133] J.R. Li, Q. Yu, E.C. Sanudo, Y. Tao, W.C. Son, X.H. Bu, Chem. Mater. 20 (2008) 1218.
[134] J. Richter, J. Schulenburg, A. Honecker, Quantum Magnetism, Springer, Berlin/Heidelberg, 2004, p. 85.
[135] B.M. Bartlett, D.G. Nocera, J. Am. Chem. Soc. 127 (2005) 8985.
[136] G. Paul, A. Choudhury, E.V. Sampathkumaran, C.N.R. Rao, Angew. Chem. Int. Ed. Engl. 41 (2002) 4297.
[137] E.Q. Gao, N. Liu, A.L. Cheng, S. Gao, Chem. Commun. (2007) 2470.
[138] O. Kahn, Molecular Magnetism, VCH Publishers Inc., New York, 1993, p. 380.
[139] J.R. Li, Q. Yu, Y. Tao, X.H. Bu, J. Ribas, S.R. Batten, Chem. Commun. (2007) 2290.
[140] P. Gütlich, H.A. Goodwin, Springer–Verlag Berlin Heidelberg, 2004, p. 1.
[141] G.J. Halder, C.J. Kepert, B. Moubaraki, K.S. Murray, J.D. Cashion, Science 298 (2002) 1762.
[142] S.M. Neville, G.J. Halder, K.W. Chapman, M.B. Duriska, P.D. Southon, J.D. Cashion, J.F. Letard, B. Moubaraki, K.S. Murray, C.J. Kepert, J. Am. Chem. Soc. 130 (2008) 2869.
[143] D. Maspoch, D. Ruiz-Molina, K. Wurst, N. Domingo, M. Cavallini, F. Biscarini, J. Tejada, C. Rovira, J. Veciana, Nat. Mater. 2 (2003) 190.
[144] M.D. Allendorf, C.A. Bauer, R.K. Bhakta, R.J.T. Houk, Chem. Soc. Rev. 38 (2009) 1330.
[145] C. Janiak, Dalton Trans. (2003) 2781.
[146] M.P. Suh, Y.E. Cheon, E.Y. Lee, Coord. Chem. Rev. 252 (2008) 1007.
[147] B.D. Chandler, D.T. Cramb, G.K.H. Shimizu, J. Am. Chem. Soc. 128 (2006) 10403.
[148] B.D. Chandler, J.O. Yu, D.T. Cramb, G.K.H. Shimizu, Chem. Mater. 19 (2007) 4467.
[149] D.T. de Lill, A. de Bettencourt-Dias, C.L. Cahill, Inorg. Chem. 46 (2007) 3960.
[150] C.A. Bauer, T.V. Timofeeva, T.B. Settersten, B.D. Patterson, V.H. Liu, B.A. Simmons, M.D. Allendorf, J. Am. Chem. Soc. 129 (2007) 7136.
[151] F. Gándara, A. de Andres, B. Gomez-Lor, E. Gutiérrez-Puebla, M. Iglesias, M.A. Monge, D.M. Proserpio, N. Snejko, Cryst. Growth Des. 8 (2008) 378.
[152] Y.Q. Huang, B. Ding, H.B. Song, B. Zhao, P. Ren, P. Cheng, H.G. Wang, D.Z. Liao, S.P. Yan, Chem. Commun. (2006) 4906.
[153] B.L. Chen, L.B. Wang, F. Zapata, G.D. Qian, E.B. Lobkovsky, J. Am. Chem. Soc. 130 (2008) 6718.
[154] B.L. Chen, L.B. Wang, Y.Q. Xiao, F.R. Fronczek, M. Xue, Y.J. Cui, G.D. Qian, Angew. Chem. Int. Ed. Engl. 48 (2009) 500.
[155] B.L. Chen, Y. Yang, F. Zapata, G.N. Lin, G.D. Qian, E.B. Lobkovsky, Adv. Mater. 19 (2007) 1693.
[156] L.G. Qiu, Z.Q. Li, Y. Wu, W. Wang, T. Xu, X. Jiang, Chem. Commun. (2008) 3642.
[157] M.D. Allendorf, R.J.T. Houk, L. Andruszkiewicz, A.A. Talin, J. Pikarsky, A. Choudhury, K.A. Gall, P.J. Hesketh, J. Am. Chem. Soc. 130 (2008) 14404.
[158] B.V. Harbuzaru, A. Corma, F. Rey, P. Atienzar, J.L. Jorda, H. Garcia, D. Ananias, L.D. Carlos, J. Rocha, Angew. Chem. Int. Ed. Engl. 47 (2008) 1080.
[159] R. Langer, Nature 392 (1998) 5.
[160] J. Salonen, A.M. Kaukonen, J. Hirvonen, V.P. Lehto, J. Pharm. Sci. 97 (2008) 632.
[161] M.G. Rimoli, M.R. Rabaioli, D. Melisi, A. Curcio, S. Mondello, R. Mirabelli, E. Abignente, J. Biomed. Mater. Res. Part A 87A (2008) 156.
[162] M. Vallet-Regí, F. Balas, D. Arcos, Angew. Chem. Int. Ed. Engl. 46 (2007) 7548.
[163] K.S. Soppimath, T.M. Aminabhavi, A.R. Kulkarni, W.E. Rudzinski, J. Control. Release 70 (2001) 1.
[164] S. Freiberg, X.X. Zhu, Int. J. Pharm. 282 (2004) 1.
[165] B. Munoz, A. Ramila, J. Perez-Pariente, I. Diaz, M. Vallet-Regi, Chem. Mater. 15 (2003) 500.
[166] P. Horcajada, C. Marquez-Alvarez, A. Ramila, J. Perez-Pariente, M. Vallet-Regi, Solid State Sci. 8 (2006) 1459.
[167] K.E. Uhrich, S.M. Cannizzaro, R.S. Langer, K.M. Shakesheff, Chem. Rev. 99 (1999) 3181.
[168] M. Vallet-Regi, A. Ramila, R.P. del Real, J. Perez-Pariente, Chem. Mater. 13 (2001) 308.
[169] P. Horcajada, C. Serre, M. Vallet-Regi, M. Sebban, F. Taulelle, G. Férey, Angew. Chem. Int. Ed. Engl. 45 (2006) 5974.
[170] T. Loiseau, C. Serre, C. Huguenard, G. Fink, F. Taulelle, M. Henry, T. Bataille, G. Férey, Chem.-Eur. J. 10 (2004) 1373.